

1,3-Diarylpyrazolyl-acylsulfonamides as Potent Anti-tuberculosis Agents Targeting Cell Wall Biosynthesis in *Mycobacterium tuberculosis*

Lutete Peguy Khonde, Rudolf Müller, Grant A. Boyle, Virsinha Reddy, Aloysius T. Nchinda, Charles J. Eyermann, Stephen Fienberg, Vinayak Singh, Alissa Myrick, Efrem Abay, Mathew Njoroge, Nina Lawrence, Qin Su, Timothy G. Myers, Helena I. M. Boshoff, Clifton E. Barry, III, Frederick A. Sirgel, Paul D. van Helden, Lisa M. Massoudi, Gregory T. Robertson, Anne J. Lenaerts, Gregory S. Basarab, Sandeep R. Ghorpade,* and Kelly Chibale*



Cite This: <https://doi.org/10.1021/acs.jmedchem.1c00837>



Read Online

ACCESS |



Metrics & More



Article Recommendations

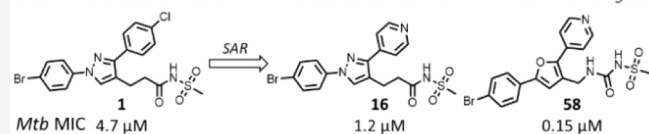


Supporting Information

ABSTRACT: Phenotypic whole cell high-throughput screening of a ~150,000 diverse set of compounds against *Mycobacterium tuberculosis* (Mtb) in cholesterol-containing media identified 1,3-diarylpyrazolyl-acylsulfonamide **1** as a moderately active hit. Structure–activity relationship (SAR) studies demonstrated a clear scope to improve whole cell potency to MIC values of <0.5 μM , and a plausible pharmacophore model was developed to describe the chemical space of active compounds. Compounds are bactericidal *in vitro* against replicating Mtb and retained activity against multidrug-resistant clinical isolates. Initial biology triage assays indicated cell wall biosynthesis as a plausible mode-of-action for the series. However, no cross-resistance with known cell wall targets such as MmpL3, DprE1, InhA, and EthA was detected, suggesting a potentially novel mode-of-action or inhibition. The *in vitro* and *in vivo* drug metabolism and pharmacokinetics profiles of several active compounds from the series were established leading to the identification of a compound for *in vivo* efficacy proof-of-concept studies.

Singleton from phenotypic screen in cholesterol media

Plausible cell-wall biosynthesis inhibitors; no cross-resistance with known cell wall targets



INTRODUCTION

Tuberculosis (TB) continues to be a global epidemic most severely affecting the underprivileged sectors of society throughout the world. According to the World Health Organization 2019 global TB report, 10 million people fell sick with TB in 2018 and 1.5 million people lost their lives.¹ The most common drug regimen currently used for the treatment of drug-sensitive TB is 40 years old and consists of four drugs—rifampicin (RIF), isoniazid (INH), pyrazinamide (PZA), and ethambutol (EMB)—taken over a minimum period of 6 months. The long treatment duration along with unpleasant side effects often lead to patient noncompliance, resulting in the development of drug-resistant TB, *viz.*, multidrug resistant (MDR) TB that is refractory to two frontline drugs RIF and INH and extensively drug resistant (XDR) TB that develops additional resistance to any fluoroquinolone and at least one of the three injectable second-line drugs (amikacin, kanamycin, or capreomycin). Treatments for drug-resistant TB are fraught with limited choices of poorly efficacious medicines with severe side effects and lengthy treatment durations of 18–24 months. Hence, there has been a strong global drive toward identifying safe new drugs with novel mode-of-actions (MoAs), which would be effective for treatment of drug-resistant TB and be included

in combination regimens aimed at treatment shortening for drug-sensitive TB. Gratifyingly, a few recently approved drugs with novel MoAs such as bedaquiline,² pretomanid,³ and delamanid⁴ have been added to the arsenal of the available TB drugs. Several follow-up drug candidates such as the DprE1 inhibitors macozinone (PBTZ-169)⁵ and TBA-7371,⁶ the MmpL3 inhibitor SQ-109,⁷ the QcrB inhibitor telacebec (Q203),⁸ and the leucyl-tRNA synthetase inhibitor GSK 3036656⁹ are in the clinical development pipeline (Figure 1). Other known drugs such as linezolid have also shown great promise in the treatment of MDR-TB and have encouraged preclinical efforts to discover safer analogues.¹⁰ Considering the significant attrition rates in clinical development and the empirical nature of the effective combination therapy toward shorter treatments, there is a continuous need to replenish the global TB drug pipeline with new bactericidal agents that avoid

Received: May 8, 2021

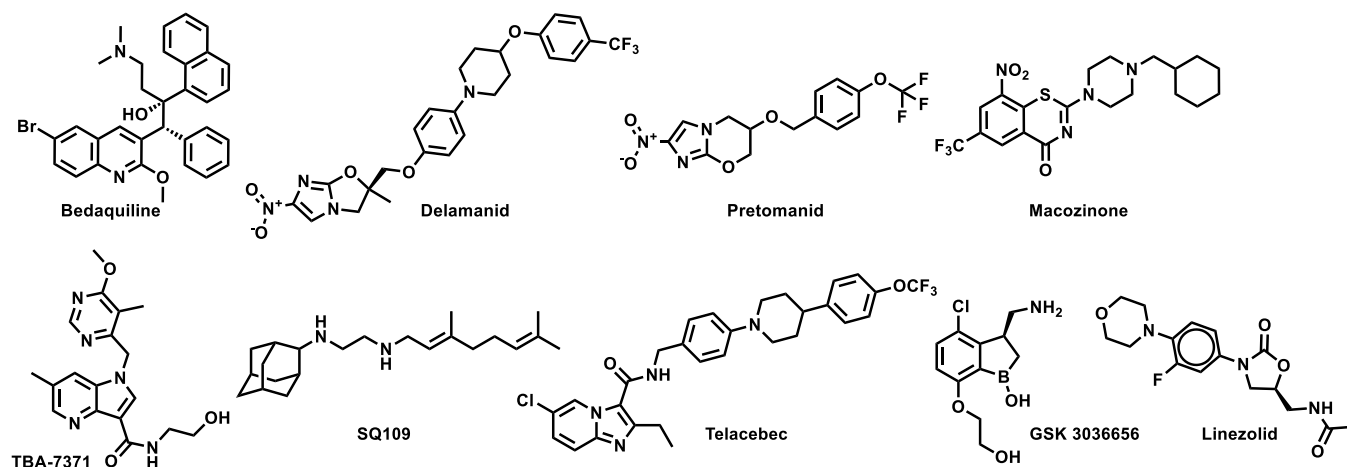


Figure 1. New approved drugs and clinical candidate for TB.

preexisting clinical drug resistance either through novel MoA or novel mode-of-inhibition (MoI) of clinically validated drug targets.

Mycobacterium tuberculosis (Mtb), the causative agent of TB, is known to adapt metabolically to the various nutrients available during its cycle of infection, persistence, and reactivation.^{11,12} Fatty acids and cholesterol are important carbon sources for *in vivo* survival and pathogenesis of Mtb,^{13,14} even though this organism can utilize carbohydrates and carbon dioxide as carbon sources and needs glucose for *in vivo* persistence.¹⁵ There have been efforts to screen compound libraries against Mtb surviving on fatty acid and cholesterol media to identify compounds efficacious against various pathological forms of Mtb.¹⁶ Herein, we report structure–activity relationship (SAR) studies and preliminary target identification studies of 1,3-diarylpyrazolyl-acylsulfonamides identified from the phenotypic screening of a compound library supplied by DuPont in cholesterol-containing media.

RESULTS AND DISCUSSION

Phenotypic Hit with a Novel MoA. A high-throughput phenotypic whole cell screen of a ~150,000 diverse set of compounds from DuPont Agrichemicals compound library against Mtb was conducted at the National Institute of Allergy and Infectious Diseases of the National Institutes of Health (NIAID/NIH, U.S.) using Mtb in two different media, Middlebrook 7H9/dipalmitoylphosphatidylcholine (DPPC)/cholesterol/bovine serum albumin (BSA)/tyloxapol (DPPC/chol) and Middlebrook 7H9/butyrate pH 6.0/nitrite/BSA/tyloxapol (butyrate pH6/nitrite). This screen identified ~2000 primary hits. The activity of these hits was confirmed by determining the minimum inhibitory concentrations (MICs) that lead to no visible growth from solid samples against Mtb under three conditions—DPPC/chol, butyrate pH6/nitrite, as well as 7H9/DPPC/casitone/tyloxapol (DPPC/cas). Of the three media used, activity in DPPC/chol medium may closely simulate *in vivo* nutritional ambience for replicating Mtb, whereas DPPC/cas is a protein-free minimal media used to identify weaker inhibitors that would be missed in standard serum containing media due to the effect of protein binding. The low pH butyrate medium containing nitrite reflects some of the environmental stresses encountered by Mtb residing in macrophages *in vivo*, namely, acidic pH of the intraphagosomal environment of the macrophage and reactive nitrite

intermediates released from nitrite.^{14,17} Among the few hits that were confirmed from the screening campaign, compound **1** was identified as a singleton with moderate activity under various media conditions; notably, it did not show any previous literature reports of antitubercular activity (Table 1).

Table 1. Hit Triage of Compound **1**^a

| | |
|---|------|
| | |
| MIC 7H9/ADC/Tw (μM) | 4.7 |
| MIC 7H9/glucose/BSA/Tx (μM) | 4.7 |
| MIC 7H9/DPPC/cholesterol/BSA/Tx (μM) | 4.7 |
| MIC 7H9/cholesterol/BSA/Tx (μM) | 4.7 |
| IC ₅₀ in 7H9/2.5 mM butyrate/pH6/0.1 mM nitrite (μM) | 6.25 |
| HepG2 IC ₅₀ glucose (μM) | >50 |
| HepG2 IC ₅₀ galactose (μM) | >50 |
| solubility (μM) | 170 |

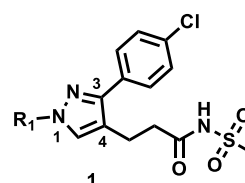
^aMIC—minimum inhibitory concentration against Mtb H37Rv; 7H9—Middlebrook 7H9; ADC—albumin-dextrose-catalase supplement; Tw—Tween 80; BSA—bovine serum albumin; Tx—tyloxapol; DPPC—dipalmitoylphosphatidylcholine; IC₅₀—50% inhibitory concentration; solubility—aqueous solubility at pH 7.4.

Though **1** has a 1,3-diarylpyrazole core found in some known anti-Mtb actives,^{18,19} it has a unique *N*-(methylsulfonyl)-propanamide substituent at the pyrazole C4 position. It had been reported as a potassium channel modulator for the treatment of a variety of human disorders.²⁰ Screening against various tool strains of Mtb indicated a novel MoA as described in the biology triage section of this manuscript. The compound was noncytotoxic against HepG2 cell line under both glucose- and galactose-containing media conditions at the highest concentration tested, minimizing the possibility of mitochondrial cytotoxicity.²¹ All these observations sparked further interest in exploring the potential of **1** to deliver a novel drug candidate for TB treatment. Detailed SAR and target identification studies were initiated as detailed in the following sections.

Synthesis. As the hit compound **1** was identified as a singleton from the screen, detailed SAR studies were needed to

identify key pharmacophoric features and to expand the SAR scope for increasing anti-Mtb activity. To this end, a systematic exploration of each substituent around the central pyrazole ring and variations of the pyrazole core were undertaken. Compounds were specifically synthesized to explore the SAR around substituents around the N1 (compounds 1–12, Table 2), C3 (compounds 13–25, Table 3), and C4 positions (compounds 26–45, Table 4). Furthermore, additional compounds were synthesized to explore replacements for the *N*-(methylsulfonyl)propanamide substituent at the C4 position

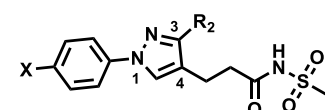
Table 2. SAR at the N1-Substituent^a



| Compound Number | R ₁ | MIC (μM) | Solubility (μM) |
|-----------------|----------------|----------|-----------------|
| 1 | | 4.7 | 170 |
| 2 | | >50 | 200 |
| 3 | | 37 | 25 |
| 4 | | >50 | <5 |
| 5 | | >50 | 165 |
| 6 | | >50 | 190 |
| 7 | | >50 | 200 |
| 8 | | 4.7 | 100 |
| 9 | | 3.1 | 50 |
| 10 | | 4.7 | 90 |
| 11 | | 25 | 75 |
| 12 | | ≥50 | 200 |

^aMICs were measured in Middlebrook 7H9/Glu/BSA/tyloxapol media; solubility was determined in aqueous pH 7.4 phosphate buffer simulating thermodynamic conditions.

Table 3. SAR at the C3 Position^a

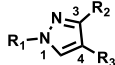


| Compound Number | X | R ₂ | MIC (μM) | Solubility (μM) |
|-----------------|----|----------------|----------|-----------------|
| 13 | Br | | 2.3 | 200 |
| 14 | Br | | 2.3 | 165 |
| 15 | Cl | | >50 | 90 |
| 16 | Br | | 1.2 | 185 |
| 17 | Br | | 6.25 | 200 |
| 18 | Br | | 20 | 196 |
| 19 | Br | | 9.4 | 60 |
| 20 | Br | | 9.4 | 200 |
| 21 | Br | | >50 | 196 |
| 22 | Br | | 50 | 200 |
| 23 | Br | | 12.5 | <5 |
| 24 | Br | | 25 | 160 |
| 25 | Br | | >50 | 200 |

^aMIC—measured in Middlebrook 7H9/Glu/BSA/tyloxapol media; solubility—aqueous solubility at pH 7.

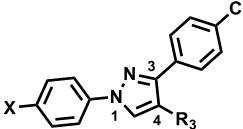
(compounds 46–50, Table 5) and to vary the central pyrazole core (compounds 51–58, Table 6).

Compounds 1–25 and 35 were synthesized by modification of the reaction sequence described previously as depicted in Scheme 1.²⁰ In short, the key intermediates, 4-formylpyrazoles (A), were synthesized by treating the appropriately substituted

Table 4. SAR at C4 *N*-Sulfonylpropanamide^a


| Compound Number | R ₁ | R ₂ | R ₃ | MIC (μM) | Solubility (μM) |
|-----------------|----------------|----------------|----------------|----------|-----------------|
| 26 | | | | >50 | 155 |
| 27 | | | | >50 | <5 |
| 28 | | | | >50 | <5 |
| 29 | | | | >50 | <5 |
| 30 | | | | >50 | 165 |
| 31 | | | | >50 | 200 |
| 32 | | | | 37 | 135 |
| 33 | | | | 12.5 | 10 |
| 34 | | | | >50 | 5 |
| 35 | | | | 6.25 | ND |
| 36 | | | | >50 | 190 |
| 37 | | | | 50 | 170 |
| 38 | | | | 4.7 | 90 |
| 39 | | | | 1.2 | 185 |
| 40 | | | | 19 | 200 |
| 41 | | | | 12.5 | 155 |
| 42 | | | | 1.2 | 195 |
| 43 | | | | 1.56 | 150 |
| 44 | | | | 3.13 | <5 |
| 45 | | | | 12.5 | ND |

^aMIC—measured in Middlebrook 7H9/Glu/BSA/tyloxapol media; solubility—aqueous solubility at pH 7.

Table 5. Heterocycles at C4^a


| Compound Number | X | R ₃ | MIC (μM) | Solubility (μM) |
|-----------------|----|----------------|----------|-----------------|
| 46 | Br | | >50 | 150 |
| 47 | Br | | 50 | <5 |
| 48 | Cl | | >50 | 200 |
| 49 | Br | | 19 | <5 |
| 50 | Cl | | 25 | 175 |

^aMIC—measured in Middlebrook 7H9/Glu/BSA/tyloxapol media at day 14; solubility—aqueous solubility at pH 7.

hydrazones with POCl₃ in a Vilsmeier–Haack formylation reaction, which was followed by a regioselective Knövenagel condensation reaction with malonic acid to obtain the corresponding *trans*-acrylic acids **B**. Selective reduction of the acrylic acids in order to avoid concomitant halogen hydrogenolysis gave the corresponding propanoic acid intermediate **C** which was coupled with methanesulfonamide in the presence of carbonyldiimidazole (CDI) and diazabicycloundecene (DBU) or, in a few cases, in the presence of dicyclohexylcarbodiimide (DCC) and dimethylaminopyridine (DMAP) to yield target compounds. The detailed synthetic schemes are described in [Supporting Information](#) (Schemes S1 and S2). Syntheses of compounds **26–41** with modified alkyl linkers at C4 are described in [Schemes S3–S6](#). Urea and carbamate derivatives **42–45** could be synthesized from common intermediate **A** via alcohols **D** and amines **E** as described in [Scheme S7](#). Syntheses of compounds **46–50** with replacement of acylsulfonamide functionality are described in [Schemes S8 and S9](#). Syntheses of compounds **51–58** with variations to the central pyrazole core are described in [Schemes S10–S14](#).

SAR at the N1-Substituent. Mtb activity measured as MIC in Middlebrook 7H9/Glu/BSA/Tx media and aqueous solubility were monitored as first tier criteria toward selection of compounds for further characterization ([Table 2](#)). Compound **2** with an unsubstituted phenyl ring showed a much higher MIC (>50 μM) relative to **1**. Replacement of *p*-bromo on the phenyl ring with *p*-fluoro, as in **3**, or moving bromine to the meta or ortho positions as in **4** and **5**, respectively, led to deterioration of activity (MICs ≥ 50 μM). Similarly, **6** with the phenyl ring replaced with 4-pyridyl and **7** with a cyclohexyl ring showed much weaker MICs (≥50 μM). Compounds **11** and **12** with polar CN and methylsulfoxide

Table 6. SAR at the Pyrazole Core^a

| Compound Number | Structure | MIC (μM) | Solubility (μM) |
|-----------------|-----------|-----------------------|------------------------------|
| 51 | | 6.25 | 200 |
| 52 | | 5.5 | 195 |
| 53 | | 37 | 135 |
| 54 | | >50 | 200 |
| 55 | | >50 | 170 |
| 56 | | 37 | 200 |
| 57 | | 19 | 90 |
| 58 | | 0.15 | 25 |

^aMIC—measured in Middlebrook 7H9/Glu/BSA/tyloxapol media; solubility—aqueous solubility at pH 7.

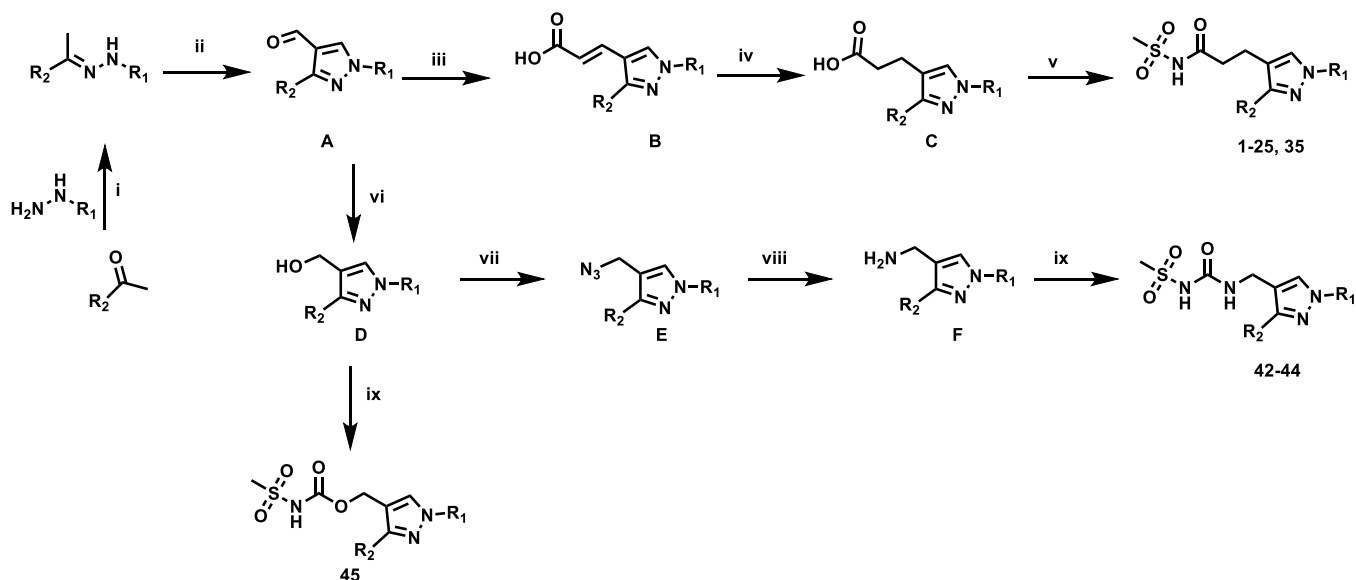
groups, respectively, at the para position of the phenyl ring showed 5–10-fold weaker activity indicating the essentiality of hydrophobic substituents at this position. Only compounds **8** and **9** with *p*-chlorophenyl and *p*-CF₃-phenyl, respectively,

retained MICs similar to **1**, albeit with lower aqueous solubility (100 and 50 μM , respectively). Compound **10** with a 4-CF₃-3-pyridyl ring at N1 showed a comparable MIC to **1** with somewhat improved solubility (90 μM) compared to **9**. Overall, variations at the N1-phenyl ring (*R*₁) demonstrated the essentiality of an aryl ring with larger hydrophobic para-substituents for Mtb activity.

SAR at the C3 Position. Compared to the N1 position, substituents at the C3 position (*R*₂) of the pyrazole showed a wider scope for structural variation leading to slightly lower MICs (Table 3). Compound **13** with a hydrogen atom in place of Cl on the C3 phenyl group retained a similar MIC to **1**. Compound **14** with *m*-Cl-phenyl also retained a similar MIC, but compound **15** with *o*-Cl-phenyl showed a >10-fold higher MIC. Compound **16** with a 4-pyridyl ring at C3 in place of Cl-phenyl improved the MIC ~4-fold, thus providing a more potent tool compound for MoA studies (see below). Compound **17** with a 3-pyridyl ring showed a MIC similar to compound **1**, and **18** with a pyrazine ring showed a 5-fold higher MIC. Compounds **19** and **20** with saturated cyclohexyl and tetrahydropyran rings, respectively, at the C3-position showed MICs similar to **1**, but **21** with a basic piperidine at C3 and its *N*-formyl derivative **22** showed much weaker activity (MICs \geq 50 μM) indicating an intolerance toward polar functionality at this position for nonaromatic *R*₂ substituents. Similarly, higher (3–5-fold) MICs were observed with **23** having a *p*-NO₂-phenyl at the C3 position and the corresponding aniline derivative **24**. Compound **25** with a C3 benzyl group also showed much weaker MIC, thus limiting the SAR scope to explore directly attached aryl, heteroaryl, and saturated rings.

SAR at C4 *N*-(Methylsulfonyl)propanamide. A few analogues were synthesized to determine the essentiality of the *N*-sulfonylpropanamide functionality linked to the pyrazole C4 position (*R*₃, Table 4). The corresponding carboxylic acid **26** and *N*-methyl amide derivative **27** showed much weaker activity (MICs > 50 μM), establishing *N*-sulfonylpropanamide as a critical functionality for potency. Methylation of the sulfonamide NH led to **28** that showed a significant decrease in activity (MIC > 50 μM) along with low aqueous solubility (<5 μM). Replacement of the carbonyl group with methylene (compound **29**) led to a high MIC (>50 μM). The data point to the need for an acidic functionality (the sulfonylpropanamide) that has specific binding interaction with the target not seen with the carboxylic acid of **26**. The specificity of the sulfonylpropanamide was further supported by swapping positions of the sulfonyl and carbonyl groups (compound **30**), leading to high MIC (>50 μM). The length of the alkyl chain linking the *N*-(methylsulfonyl)carbamoyl group to the pyrazole core was also critical to maintain lower MICs as demonstrated with **31** (MIC > 50 μM) and **32** (MIC 37 μM) having shorter and longer linking alkyl chains to the pyrazole C4 position. The ethyl sulfonyl analogue **33** showed a 4-fold higher MIC, while the larger cyclopropylsulfonyl group was even less active (MIC > 50 μM) indicating a limited scope around the sulfonyl alkyl group. Hence, *N*-(methylsulfonyl)-propanamide represents an optimal pharmacophore predicted to engage in key interactions with the target as delineated later.

Modifications on the propanamide chain were then explored to better understand SAR and continue compound optimization, particularly to improve metabolic stability of the acylsulfonamide while maintaining the potency of the compounds [refer drug metabolism and pharmacokinetics

Scheme 1. General Synthetic Scheme^a

^aReagents and conditions: (i) KOAc, EtOH, 80 °C; (ii) POCl₃, DMF, 80 °C; (iii) malonic acid, piperidine, pyridine, 90 °C; (iv) method 1: NH₂NH₂·H₂O, MeOH, 80 °C; method 2: NBSH, Et₃N, THF, 45 °C; (v) method 1: CH₃SO₂NH₂, CDI, DBU, DMF, 90 °C; method 2: CH₃SO₂NH₂, DCC, DMAP, 0–45 °C; (vi) NaBH₄, MeOH, 25 °C; (vii) PPh₃, DIAD, NaN₃, H₂SO₄, DCM, 0 °C to 25 °C; (viii) PPh₃, THF/H₂O, 60 °C; (ix) CDI, methanesulfonamide, DIPEA, DCM, dichloroethane, or DMF depending on the solubility of the substrate, 25–90 °C.

(DMPK) section]. Addition of a methyl group either on α - or β -carbons of the propanamide chain led to compounds **36** and **37** with much weaker activity (MICs ≥ 50 μ M) compared to the unsubstituted analogue **35** (MIC 6.25 μ M), indicating a likely clash at the target level or perturbation of the preferred side chain binding conformation. Comparatively, better MICs were observed by constraining the methyl group into a cyclopropane ring as in **40** and **41** (MICs 12.5–19 μ M). The *trans*-acrylamide derivatives **38** and **39** showed more potent MICs (1.2–4.7 μ M). Compounds **42**, **43**, and **44** with a sulfonylurea tethered to C4 and a net replacement of CH₂ with NH showed lower MICs compared to the corresponding *N*-(methylsulfonyl)propanamide derivatives, indicating a possible H-bond donor interaction from the urea NH with the target. Compound **45** with a sulfonylcarbamate functionality showed an 8-fold higher MIC relative to **43**, supporting the hypothesis that there is a contribution to binding by the urea NH.

Further, we explored replacing the *N*-acylsulfonamide group with another functionality envisioned to similarly position an acidic group (Table 5). Compounds **46** and **47** with tetrazole and 1,2,4-oxadiazolone moieties attached to C4 *via* an ethyl linker and compound **48** with a pyrimidinetrione attached *via* a methylene linker showed much higher MICs (≥ 50 μ M). Only **49** with an 1,3,4-oxadiazolone attached *via* an ethyl linker at the C4 position showed a lower MIC, about 4-fold higher than **1**, albeit the low solubility (< 5 μ M) rendered the compound less interesting. Overall, there is a limited scope for replacement of the *N*-acylsulfonamide functionality. Compound **50** wherein the propanamide was cyclized into a dihydroisoxazole ring also retained an MIC within 4-fold of compound **1**. Further scope for optimization of MICs using C4 functionalities as in compounds **49** and **50** by varying other substituents in the molecule remains to be explored.

SAR of the Pyrazole Core. Table 6 shows the analogues synthesized to understand the importance of the relative positions of substituents on the pyrazole ring and the influence

of alternative isosteric heterocycles. Compounds **51** and **52** retained the same relative position of all three substituents and the pyrazole nitrogen lone pair of **1** and **3** and, not surprisingly, showed similar MICs. Analogues **53** and **54** with 1,4-diarylpyrazole and 3,5-diarylpyrazole cores also display the three substituents in the same relative orientation as **1** but shift the position of the pyrazole nitrogen lone pair resulting in much higher MICs (≥ 50 μ M) and indicating an important target interaction for the pyrazole N2 of **1**. 1,5-Diarylpyrazole **55** had a much higher MIC (≥ 50 μ M) further confirming the importance of relative positions of aryl rings in maintaining potency. Replacement of the pyrazole with other five-membered heterocycles as with **56** and **57** having oxazole and thiazole cores, respectively, showed 5–8-fold weaker MICs. Compound **58** with a furan core showed much more potent activity with MIC below 0.5 μ M. The above observations indicate a smaller angle between the R1 and R2 substituents of the smaller pyrazole, and furan heterocycles (150.3 and 125.5°, respectively) are favored over what would be seen with the larger thiazole core (154.6°) in **57**. Loss of potency for oxazole **56** is consistent with the observation that polar atoms are not well tolerated at the other position of the five-membered ring as seen for **53** and **54**. The furan oxygen is favorable as is the 2-position N of the pyrazole of **1** and of **51**. Improved activity of furan analogue **58** could be attributed to O being more electronegative than N, possibly making a stronger hydrogen-bonding interaction with the target.

The above SAR demonstrates the specific structural requirements of compound **1** and the analogues required to maintain anti-Mtb activity alluding to specific target engagement by the scaffold.

Representative Pharmacophore. We have accordingly developed a pharmacophore hypothesis to summarize key structural features of the scaffold that may aid in efforts to further optimize this series. To describe the chemical space of the active acyl sulfonamide pyrazole compounds, a series of

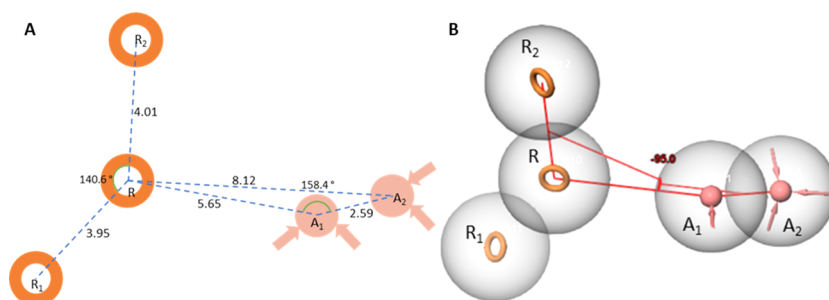


Figure 2. Representations of the AARRR pharmacophore model. (A) 2D representation of the pharmacophore model with two of the ring features (R_1 and R_2) both shown to be about 4 Å from the central R feature forming an angle of 140° with each other. The first acceptor feature (A_1) lies 5.65 Å from R with the acceptor feature A_2 lying an additional 2.59 Å from A_1 forming an angle of 158.4° with A_1 and R. (B) 3D representation of the pharmacophore model showing the A_1 and A_2 features to be out of the plane formed by R, R_1 , and R_2 with a -95.0° dihedral angle around a line from R to A_1 .

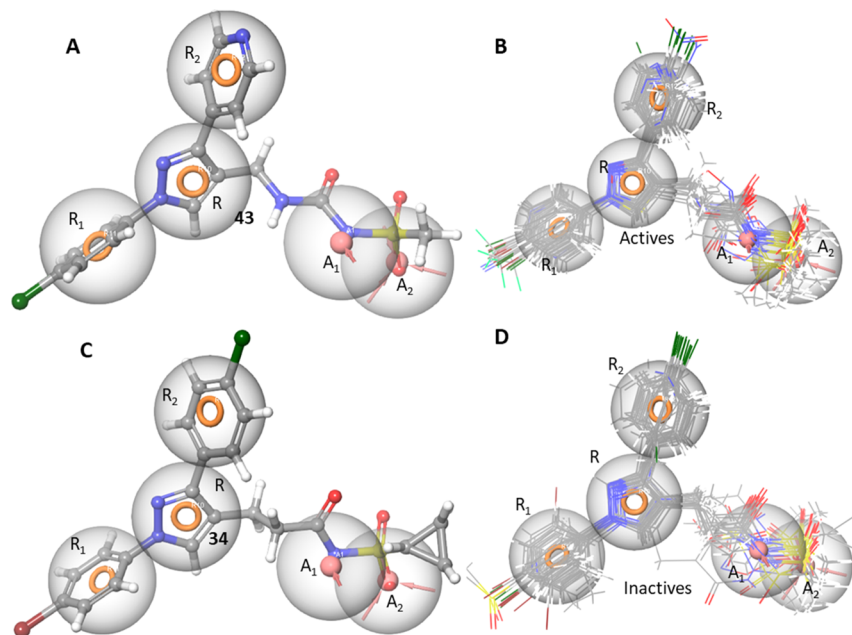


Figure 3. (A) Compound 43 fitted to the five-feature AARRR pharmacophore hypothesis very closely. The three aromatic ring features are occupied by the chlorophenyl, pyrazole, and pyridyl groups, while the deprotonated sulfonamide fits the negative charge feature and sulfone O fits the acceptor feature; (B) an overlay of all active compounds in this set closely fitting all five pharmacophore features. (C) Compound 34 is an example of an inactive compound, *i.e.*, an excellent fit of the pharmacophore. This loss in activity is brought about by the bulky cyclopropyl group extending into a region outside of the pharmacophore. This region could be defined as an excluded volume. (D) Inactive compounds from this set either fit the pharmacophore hypothesis fully or partially with many occupying spaces outside the definition of the pharmacophore, suggesting potential for the definition of excluded volumes past the A_2 feature and between the A_1 and R_1 features.

pharmacophore hypotheses were generated from the set of compounds using the phase module from the Schrodinger molecular modeling suite.²² The activity cutoff was defined as MIC < 25 μ M in the 7H9/glucose/BSA/Tx assay among the set of 58 compounds in this series. An AARRR (A-acceptor, R-ring) pharmacophore hypothesis (Figure 2) consisting of three aromatic rings (R , R_1 , and R_2) and two hydrogen bond acceptors was found to best describe the chemical space of active compounds. A central aromatic ring feature (R) corresponds to the central pyrazole core with two more aromatic ring features corresponding to aromatic substitutions at the 1 and 3 positions (R_1 and R_2 , respectively). The first acceptor feature (A_1) can be found approximately 5.65 Å from the C4 position of the pyrazole core fitting the negatively charged N of the acyl sulfonamide moiety. At physiological pH, the acyl sulfonamide NH is deprotonated, creating an anion that could serve as a hydrogen bond acceptor. The second

acceptor (A_2) lies another 2.43 Å away forming a 158° angle between A_1 and the central ring feature (Figure 2A). A_1 moves out of the plane formed by the three ring features forming a 95° dihedral angle around a line connecting the R feature and the A_1 feature (Figure 2B). In this set of compounds, R_1 often seems, at a minimum, to require negatively charged acid groups as only compounds with a pK_a below physiological pH have shown activity.

A representative active compound 43 fits all five of these features very closely (Figure 3A). The pharmacophore fit of each ligand was determined *via* phase docking with the fit evaluated using the phase fitness score.²² All active compounds featured in this manuscript fit the five features (Figure 3B) very closely.

A bioisostere replacement of the acyl sulfonamide with the 1,3,4-oxadiazolone of 49 introduces an acid center with a predicted²³ pK_a of 7.87 ± 0.4 in contrast to the predicted pK_a

Table 7. MICs Against Isogenic Single-Drug Resistant Mutant Strains of Mtb^a

| Mtb strain | MIC (μ M) | | | | | | |
|------------------------|----------------|------|-------|-------|-------|-------|------|
| | 1 | 8 | 43 | 58 | RIF | INH | ETH |
| H37RvMA | 4 | 4 | 0.5 | 0.24 | 0.002 | 7.8 | 15.6 |
| Δ <i>cyd</i> | 4 | 4 | 0.5 | 0.12 | 0.005 | | |
| QcrB ^{A317T} | 4 | 4 | 0.5 | 0.12 | 0.005 | | |
| MmpL3 ^{G253E} | 4 | 4 | 1 | 0.24 | 0.005 | | |
| MmpL3 ^{G758A} | 2 | 2 | 1 | 0.5 | 0.004 | | |
| DprE1 ^{Y314C} | 3 | 4 | 2 | 0.24 | 0.005 | | |
| DprE1 ^{P116S} | 0.5 | 0.5 | 0.12 | 0.12 | 0.002 | | |
| DprE1 ^{T314H} | 0.5 | 0.5 | 0.12 | 0.12 | 0.002 | | |
| InhA-OE | 0.4 | 0.24 | <0.12 | <0.13 | 0.001 | 31.2 | |
| KatG ^{T198A} | 15.6 | 15.6 | 4 | 1 | 0.003 | >62.5 | >125 |
| EthA ^{C253R} | 8 | 8 | 2 | 0.5 | 0.002 | 7.8 | >125 |

^aInhA-OE: InhA overexpressor (H37Rv-LP:*fabG1/inhA-c-15t*); RIF: rifampicin; INH: isoniazid; ETH: ethionamide.

of the sulfonamide of **43** of 3.72 ± 0.23 , thus lowering the propensity for an acceptor/negative charge to form at physiological pH. Since the oxadiazolone has a pK_a close to physiological pH, both the protonated and deprotonated states need to be considered. Only the deprotonated form fits all five features of the pharmacophore hypothesis. This poorer fit explains the weaker MIC (19μ M) of **49** compared to **43** (1.56μ M) (Figure S1c).

Compounds **28–31** were all inactive with poor pharmacophore fits for at least one reason as explained in the supplementary section with Figure S1. Compounds **33** and **34** (Figure 3C) with their respective ethyl and cyclopropyl attachments to the sulfone and **36** and **37** with methyl groups in positions α and β to the pyrazole core all showed near perfect fits for the pharmacophore model despite a complete loss of activity. These compounds contain additional bulk occupying regions not defined by the pharmacophore suggesting potential excluded volumes. Excluded volumes beyond the A_2 feature and adjacent to the alkyl linker at the sites of potential branching would penalize these compounds. These excluded volumes would need more examples to be properly defined. An overlay of all inactive compounds presented in the study (Figure 3D) demonstrates many of them to occupy regions that could be considered for excluded volumes.

Compound **58** with a furan core fulfills all pharmacophore features (Figure S1d) and showed potent activity, whereas compounds **53**, **54**, and **56** with changes in the core ring (R) are examples of weak actives with good fits. Comparing the matched pair of inactive **53** and active **51** would suggest that a heteroaromatic acceptor N contributes to activity. However, small changes to the π -characteristics of the core caused by these rearrangements may also contribute to the lower activity. More data from analogues containing rearrangements of this core would be needed to confirm the contribution of this acceptor and warrant expanding the definition of this pharmacophore feature to include an acceptor corresponding to the 2-position of the pyrazole core.

Biology Triage. Compounds **1**, **8**, **43**, and **58** were screened against various tool strains of Mtb to deconvolute the MoA for anti-Mtb activity. None of the compounds showed modulation in MICs against a cytochrome *bd* oxidase knockout mutant strain (Δ *cyd*)^{24,25} nor against a QcrB mutant (QcrBA317T), thereby eliminating the two targets of the respiratory pathway as a likely target (Table 7). Neither did the compounds elicit a positive response in the *PrecA*-LUX

bioluminescence reporter assay,²⁶ which is designed to detect modulation in the *recA* expression, an indicator of DNA damage, hence ruling it out as a MoA for the compounds (Figure S2 in the Supporting Information). However, the compounds showed sustained signals in the *PiniB*-LUX bioluminescence reporter assay that detects modulation in the *iniBAC* operon expression,²⁶ an indicator of cell wall biosynthesis being disrupted (Figure S3). The prediction that the compounds inhibited cell wall biosynthesis was further confirmed by transcriptional profiling studies that showed upregulation in the genes involved in the cell wall biosynthesis, including many of the genes upregulated by INH such as *acpM*, *fabD*, *kasA*, *kasB*, *accD6*, *rv2248*, *efpA*, *iniB*, *iniA*, and *iniC* (Tables S3 and S4 in the Supporting Information). Despite these similarities, some of the genes that were upregulated during INH treatment (*ppsA*, *ppsB*, *ppsC*, *ppsD*, *ppsE*, and *fbpC2*) were downregulated during exposure to compounds **8** and **16**, indicating differences in transcriptional responses. The compounds were screened against the mutant strains of MmpL3 and DprE1 which frequently encountered cell wall targets (Table 7). Two strains carrying a mutation in MmpL3 (*G253E* or *G758A*) were not resistant, arguing against MmpL3 as the target. Similarly, three strains carrying mutations in DprE1 (*Y314C*, *P116S*, or *T314H*), which confer resistance to other DprE1 inhibitors, were not resistant, suggesting that DprE1 is not the target. In addition, other isogenic single-drug resistant strains of known cell wall targeting drugs such as INH and ethionamide (ETH) were also not cross-resistant to the compounds (Table 7). Taken together, these data suggest a MoA that most likely involves interference with Mtb cell wall biogenesis in a manner that does not lead to cross resistance to other cell wall inhibitors. Studies to determine the specific MoA of this series are underway.

Bactericidal Activity Against Clinical Isolates. The bactericidal activity of representative compounds **1**, **8**, and **43** against replicating Mtb was evaluated through the exposure of Mtb cultures to various concentrations of compounds for 8 days and allowing the treated cultures to regrow on fresh media after washing out the excess free drug (Figure S4 in the Supporting Information). All tested compounds showed 2–2.5 log CFU reduction at 1–4 \times MIC concentrations within 8 days, indicating the bactericidal nature of the compounds. However, the compounds were not active against non-replicating Mtb under nutrient starvation conditions. Compound **16** retained activity against three drug-sensitive, two

Table 8. MICs of Compound 16 Against Clinical Mtb Isolates

| Mtb isolate | resistant profiles | MIC of compound 16 (μM) ^a |
|-------------|---|---|
| H37RvMa | susceptible | ≤ 15 |
| S2371 | susceptible | 30 |
| S1125 | susceptible | 15–30 |
| MD55 | MDR: INH; RMP; EMB; PZA; SM | 60 ^b |
| MD96 | XDR: INH; RIF; AM; KM; CAP; OFLX; EMB; ETH; PZA; SM | ≤ 30 ^b |
| R88 | INH mono-resistant | 30 ^b |
| R296 | MDR: INH; RIF; EMB; ETH | 60 ^b |
| R3027 | RIF mono-resistant | 60 ^b |

^aMICs were determined by the MIGIT method. ^bValues within 4-fold of MICs against drug-susceptible isolate are considered sensitive to the test compound; INH: isoniazid; RIF: rifampicin; AM: amikacin; KM: kanamycin; CAP: capreomycin; OFLX: ofloxacin; EMB: ethambutol; ETH: ethionamide; PZA: pyrazinamide; SM: streptomycin.

Table 9. *In Vitro* and *In Vivo* DMPK Parameters^a

| compound | TPSA | log <i>D</i> | microsomal clearance remaining | H/R/M % | Human PPB <i>f</i> _u | <i>t</i> _{1/2} terminal (h) | <i>V</i> _d (L/kg) | CL _b (mL/min/kg) | CL _u (mL/min/kg) | AUC _{0–t} (min $\mu\text{mol/L}$) |
|----------|-------|--------------|--------------------------------|---------|---------------------------------|--------------------------------------|------------------------------|-----------------------------|-----------------------------|---|
| 1 | 81.1 | 2.4 | 90/74/71 | | 0.004 | 2.0 | 0.2 | 1.18 | 295 | 3527 |
| 8 | 81.1 | 2.0 | 98/>99/87 | | 0.023 | 3.6 | 1.2 | 2.56 | 111 | 4883 |
| 10 | 93.9 | 1.87 | 94/98/94 | | 0.036 | 3.0 | 8.7 | 67.4 | 1872 | 134 |
| 16 | 93.9 | 0.93 | 85/94/79 | | 0.009 | 1.3 | nd | >200 | >20000 | 15 |
| 17 | 93.9 | 0.84 | 37/95/94 | | 0.022 | 1.7 | 28.1 | 178 | 8091 | 31 |
| 20 | 90.3 | 0.55 | 86/83/77 | | 0.07 | 2.3 | 29.3 | 145 | 2071 | 31 |
| 38 | 93.9 | 0.98 | 88/82/85 | | 0.015 | 1.1 | nd | >200 | >20000 | 8.7 |
| 40 | 93.9 | 1.06 | >99/92/96 | | 0.01 | 0.9 | nd | >200 | >20000 | 21 |
| 43 | 106 | 0.81 | 99/98/91 | | 0.041 | 2.0 | nd | >200 | >4878 | 29 |
| 45 | 103.2 | 2.73 | 97/97/98 | | 0.03 | 5.8 | nd | >200 | >20000 | 22 |
| 51 | 81.1 | 2.1 | >99/87/91 | | 0.01 | 3.6 | 1.0 | 3.13 | 313 | 1359 |
| 58 | 101.6 | 0.36 | 98/87/85 | | 0.007 | Nd | nd | >200 | >20000 | 20 |

^a*In vivo* mouse PK parameters calculated from the noncompartmental analysis of intravenous dosing at 2 mg/kg; TPSA: total polar surface area; H/R/M: human/rat/mouse; PPB: plasma protein binding; *f*_u: fraction unbound; *V*_d: Volume of distribution; CL_b: total body clearance determined from whole blood; CL_u: unbound blood clearance determined from CL_b and plasma protein binding (assuming blood to plasma ratio of 1). AUC: area under the curve; nd: not determined.

monodrug resistant, and three MDR/XDR clinical isolates of Mtb, indicating potential utility of the compounds from the series to treat drug-sensitive as well as drug-resistant TB (Table 8). The MIGIT (mycobacteria growth indicator tube) assay uses higher inoculum in liquid broth designed for faster growth of mycobacteria and involves longer incubation times relative to the Alamar Blue MIC microtiter plate assay used for the SAR investigation herein.²⁷ Hence, MIC values between the two assays will not be comparable. Nonetheless, it is gratifying that the MIC shifts between MDR and susceptible Mtb strains in the MIGIT assays were relatively small (less than 4-fold), thereby suggesting broader clinical utility.

***In Vitro* and *In Vivo* DMPK Profiles.** In general, the compounds in the series showed moderate-to-good metabolic stability in mouse, rat, and human microsomes as presented in Table 9. The high plasma protein binding (PPB) observed for the compounds may be attributed to high albumin binding associated with the acidic acylsulfonamide functionality along with the high degree of lipophilicity. Compound 20 showed lower protein binding presumably due to lower lipophilicity imparted by the tetrahydropyran ring attached to the C3 position. The compounds in Table 9 were also profiled for *in vivo* pharmacokinetics (PK) following intravenous dosing in mice.

The hit compound 1 had a low *in vivo* mouse blood clearance (CL_b) and a low volume of distribution (*V*_d) that translated to high *in vivo* exposure. Replacing the N1 aryl group with a 4-CF₃-3-pyridyl ring in 10 led to a dramatic increase in

clearance and consequently lower exposure. Rapid CL_b values were also observed for 16 and 17 with 4-pyridyl and 3-pyridyl groups, respectively, at the C3 position. The rapid *in vivo* clearance of these compounds was all the more problematic due to the relatively high PPB leading to exceedingly high unbound clearance (CL_u) values calculated by correcting CL_b for plasma-free fraction (assuming blood-to-plasma ratio of 1).²⁸ *In vivo* metabolite identification studies of 17 revealed that the high clearances were in part due to hydrolysis of the acylsulfonamide (data in Supporting Information). Subsequent SAR exploration therefore focused on modifications that were designed to increase stability of the acylsulfonamide while maintaining the potency of the compounds. However, neither addition of a double bond to the acyl chain (38) nor cyclopropanation (40), replacement of the sulfonamide with a sulfonylurea (43), or sulfonylcarbamate (45) improved the clearances of the compounds. In addition, except for 10 which had a N1 CF₃-3-pyridyl ring, all pyridyl compounds had total clearances that exceeded hepatic blood flow in mice (90 mL/min/kg), which suggests that extra-hepatic metabolism may be a significant mechanism of clearance. The high total polar surface area (TPSA) and the low log *D* of these pyridyl derivatives (Table 7) suggest that the compounds have low lipoidal permeability, and it is therefore likely that transporter-mediated clearance was also a key contributor to the observed total clearance.^{29,30} This was further validated by performing *in vivo* metabolite identification studies on 43. Following intravenous dosing of the compound in mice, only unchanged

compound was detected in blood, urine, and feces, suggesting that metabolism was not a major contributor to its clearance. Compounds, 1, 8, and 51 had high exposure on oral dosing (data not shown), with 8 in particular showing almost complete absorption (bioavailability > 95%) even at high doses. This compound therefore had the best balance of *in vitro* potency and *in vivo* PK and was therefore selected for further *in vivo* proof-of-concept studies.

In Vivo Efficacy. *In vivo* efficacy testing was performed at an oral dose of 200 mg/kg in the acute Balb/c mouse model to evaluate the ability of 8 to inhibit replicating intracellular Mtb in lungs.^{31–34} Treatment was initiated 7 days after a low-dose aerosol infection with Mtb Erdman pFCA LuxAB strain³² and continued for 12 consecutive days. The compound was well tolerated during the treatment period but was not efficacious in reducing Mtb lung burdens in treated mice relative to the untreated mice as measured by quantification of relative light units of the luciferase expressing Erdman strain from the lung homogenate or by CFU counts obtained by plating serial dilutions of the lung homogenate on agar plates. As a positive control, EMB at 100 mg/kg once a day led to a 2-log CFU reduction in this model. To explain the results, free oral exposure of compound 8 in healthy mice at 200 mg/kg oral dose was compared with the MIC against the Mtb Erdman strain used for the efficacy studies (9.1 μ M) and the inhibitory concentration against intracellular Mtb (IC₉₀ = 11 μ M) (Figure 4). In-study PK performed on the last 2 days of

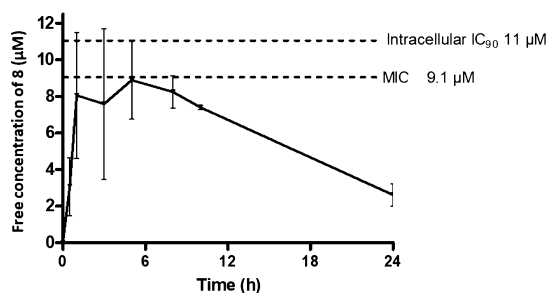


Figure 4. Free exposures of 8 (calculated using human PPB) following a single oral dose of 200 mg/kg in mice.

treatment matched closely with the healthy PK (data in the Supporting Information). From the two analyses, it is evident that compound 8 at 200 mg/kg failed to achieve drug exposures necessary to exert an antimicrobial effect *in vivo*. While much higher or more frequent dosing may provide sufficient exposure to demonstrate efficacy, the underlying data suggest that further optimization of antibacterial activity and/or PK is required to do so at lower doses that would feasibly predict human utility. Work toward achieving these improvements is in progress and will be reported in a future manuscript.

CONCLUSIONS

In summary, phenotypic screening of a DuPont compound library against Mtb in cholesterol-containing media identified 1,3-diarylpyrazolyl-acylsulfonamide 1 as a moderately active hit with a potentially novel MoA. The SAR studies described here demonstrate a clear scope to improve the MICs of compounds to <0.5 μ M, and a plausible pharmacophore model was developed to summarize SAR of the series and describe the chemical space of active compounds. Screening of the

compounds against a panel of various tool strains of Mtb ruled out the involvement of known mechanisms and/or targets such as DNA damage and respiration but suggested involvement of cell wall damage in the MoA. RNA microarray studies of Mtb cultures treated with the compounds confirmed the upregulation of genes that are involved in lipid metabolism/fatty acid biosynthesis. Isogenic single-drug resistant mutant strains of MmpL3, DprE1, InhA, and EthA were not cross-resistant with the compounds, indicating novel MoA or perhaps an alternative MoI of the targets. The compounds are bactericidal against replicating Mtb and retain activity against MDR clinical isolates of Mtb. These features make the series an attractive chemical matter for further target identification and drug discovery efforts to potentially identify a novel clinical candidate for treatment of TB. Further drug optimization work is needed to improve upon both the Mtb activity of the series and *in vivo* PK if compounds with efficacy in TB models of infection are to be realized.

EXPERIMENTAL SECTION

MIC Testing and Bioluminescence Reporter Assay. MIC determinations were done as previously described.³⁵ INH was included as a positive control. Briefly, Mtb H37Rv (ATCC 27294) was grown in Middlebrook 7H9/Glu/BSA/tyloxapol consisting of Middlebrook 7H9 broth base (4.7 g/L)/BSA fraction V (5 g/L)/dextrose (4 g/L)/NaCl (0.81 g/L)/0.05% tyloxapol to an OD_{650nm} of 0.2, at which stage the cells were diluted 1000-fold in the same medium. The compound was serially diluted in Middlebrook 7H9/Glu/BSA/tyloxapol medium in round-bottom 96-well plates (Nunc) at 50 μ L/well followed by addition of an equal volume of diluted cell suspension. Plates were incubated in sealed bags at 37 °C, and growth was recorded after 1 and 2 weeks of growth using an enlarged inverted mirror. The MIC was recorded as the compound concentration that completely inhibited all visible growth. Bioluminescence reporter assays were carried out as described by Naran *et al.*²⁶

MICs Against Mutant Strains. Alamar Blue fluorescence-based broth microdilution assay was used to assess the MICs of compounds against Mtb mutant strains, as described previously.³⁶ MICs were determined after 7 days of growth in standard Middlebrook 7H9/glycerol/ADC/Tween-80. For QcrB and *cydA* mutants, the growth measurement was monitored by OD₆₀₀. MIC was defined as the concentration required to inhibit growth by 90%.

RNA Extraction and Transcriptional Profiling. RNA extraction from Mtb H37Rv (ATCC 27294) grown to an OD₆₅₀ of 0.2 and subsequently treated for 6 h with 1× and 10× MIC of compound or vehicle control was performed using previously described methods.³⁷ RNA was also extracted from control cultures treated for 6 h with INH (2 μ M) or solvent control. RNA (4 mg) yielding an RNA integrity number of 8 or higher, as determined by the Agilent 2100 Bioanalyzer, was subsequently used for fluorescent-tagged cDNA synthesis with a random hexamer (4.5 mg) (Invitrogen) in a final volume of 14.5 μ L by sequential heat denaturation at 70 °C for 5 min, cooling on ice, and addition of 5 μ L of 5× First-Strand buffer, 1.25 μ L of 0.1 M DTT, 2.5 μ L of dNTP mix (consisting of 5 mM each of dATP, dGTP, dTTP, and 0.5 mM dCTP), 1 μ L of 200 U/ μ L SuperScriptIII (Invitrogen), 1 μ L of 40 U/ μ L RNaseOut, and 1 μ L of Cy3 or Cy5-dCTP (GE) with incubation at 25 °C for 5 min and at 48 °C for 90 min. RNA was removed by adding 5 μ L of 1 M NaOH followed by incubation at 70 °C for 15 min. After neutralization with 5 μ L of 1 M HCl, fluorescent cDNA was purified on an Amicon Ultra-0.5 column (Millipore) according to the manufacturer's recommendations. Fluorescent cDNA was analyzed with a NanoDrop ND-1000 spectrophotometer. Equal amounts (0.7 μ g) of Cy3- and Cy5-labeled cDNA were hybridized to the Agilent SurePrint G3 4 × 44K custom oligonucleotide microarrays (design number 021966, 021362) in the TECAN HS Pro 4800 hybridization station. Hybridization was

performed using Agilent 2× Gene expression hybridization HI-RPM buffer and 10× Blocking Reagent at 65 °C for 17 h. Arrays were washed with Agilent Gene Expression Wash Buffer 1 at room temperature and Gene Expression Wash Buffer 2 at 37 °C. Slides were dried under nitrogen gas for 3 min at 30 °C and imaged using an Agilent high-resolution DNA microarray scanner (model G2505C) at 5 μm resolution and 100/10% PMT dual scanning for XDR extended dynamic range. Agilent Feature Extraction software was used for image analysis.

Pharmacophore Hypothesis Generation. To generate the pharmacophore hypothesis, all compounds in this set were prepared using Maestro 12.4³⁸ to generate minimized 3D structures and determine the most likely protonation state at biological pH. A pharmacophore model was then developed using the Phase Develop Pharmacophore Model tool.²² The pharmacophore model was created from multiple ligands with the active ligands defined by an activity cutoff of MIC < 25 μM in the 7H9/glucose/BSA/Tx assay. The find best alignment method was chosen with the default hypothesis settings of four to five features and all default pharmacophore features allowed. The pharmacophore hypotheses generated were then inspected, and the hypothesis that best represented the dataset was selected and validated against a wider set of compounds from this series.

DMPK. All protocols for *in vitro* DMPK studies and mouse PK studies are available in the [Supporting Information](#). Animal studies were conducted following guidelines and policies as stipulated in the UCT Research Ethics Code for Use of Animals in Research and Teaching after review and approval of the experimental protocol by the UCT Senate Animal Ethics Committee (protocol FHS-AEC 013/032).

Chemistry. All commercial reagents were purchased from Sigma-Aldrich, Combi-Blocks, Enamine, or Fluorochem and were used without further purification. Solvents were used as received unless otherwise stated. Analytical thin-layer chromatography was performed on SiO₂ plates on aluminum backing. Visualization was accomplished by UV irradiation at 254 and 220 nm. Flash column chromatography was performed using a Teledyne ISCO flash purification system with SiO₂ 60 (particle size 0.040–0.055 mm, 230–400 mesh). Purity of all final derivatives for biological testing was confirmed to be >95% as determined using an Agilent 1260 Infinity binary pump, Agilent 1260 Infinity diode array detector (DAD), Agilent 1290 Infinity column compartment, Agilent 1260 Infinity standard autosampler, and Agilent 6120 quadrupole (single) mass spectrometer equipped with APCI and ESI multimode ionization source using a Kinetex Core C18 2.6 μm column (50 mm × 3 mm), mobile phase B of 0.4% acetic acid, 10 mM ammonium acetate in a 9:1 ratio of HPLC grade methanol, and type 1 water, mobile phase A of 0.4% acetic acid in 10 mM ammonium acetate in HPLC grade (type 1) water with a flow rate of 0.9 mL/min, and DAD; or an Agilent UPLC–MS was used: Agilent Technologies 6150 quadrupole, ES ionization, coupled with an Agilent Technologies 1290 Infinity II series UPLC system Agilent 1290 series HPLC at two wavelengths 254 and 290 nm using the following conditions: Kinetex 1.7 μm Evo C18 100A, LC column 50 mm × 2.1 mm, solvent A of 0.1% (formic acid) water, and solvent B of 0.1% (formic acid) acetonitrile. The structures of the intermediates and final products were confirmed by ¹H NMR and mass spectrometry. ¹H NMR spectra were recorded on a Bruker spectrometer at 300 or 400 MHz. Chemical shifts (δ) are given in ppm downfield from TMS as the internal standard. Coupling constants, *J*, are recorded in hertz (Hz). Synthesis details and data of intermediates are supplied in [Supporting Information](#) (Section 1).

General Sulfonamide Coupling Procedure for the Synthesis of Compounds 1–25, 27–29, 31–41, and 51–57. **Method 1: CDI-Mediated Sulfonamide Coupling.** To a solution of the appropriate acid (1 equiv) in *N,N*-dimethylformamide (DMF) was added CDI (2 equiv), and the resulting reaction mixture was stirred for 10 min at 50 °C. Then, the appropriate sulfonamide (1.2 equiv) and DBU (1.2 equiv) were added, and the resulting reaction mixture was heated to 90 °C for 16–48 h. The reaction mixture was then cooled to 25 °C, water was added (30 mL), and the aqueous layer was extracted with

EtOAc (3×). The combined organic layers were dried over Na₂SO₄ and concentrated *in vacuo*. The crude reaction mixture was purified by flash chromatography using ISCO Teledyne on a 12 g RediSep Rf column and elution using a gradient of the appropriate solvent mixtures to yield the desired products.

Method 2: DCC-Mediated Sulfonamide Coupling. To the solution of the appropriate acid (1.00 equiv) and methanesulfonamide (1.20 equiv) in DMF were added DCC (2.50 equiv) and DMAP (1.50 equiv). The reaction mixture was stirred at 30–40 °C for 16–48 h. The reaction mixture was quenched with water (5 mL), and pH was adjusted to 6 with 1 N HCl. The aqueous phase was extracted with EtOAc (3×). The organic phase was washed with brine, dried over Na₂SO₄, and concentrated *in vacuo*. The residue was purified by a silica gel column or preparative HPLC chromatography to yield the appropriate compound.

Method 3: Acid Chloride Coupling with Sulfonamide. To a solution of appropriate sulfonamide (5 equiv) in dichloromethane (DCM) was added Et₃N (5–10 equiv). Then, the appropriate acyl chloride (1 equiv) was added at 0 °C. The mixture was stirred at 15 to 25 °C for 16–24 h. The mixture was poured into 1 N HCl and extracted with DCM. The combined organic phase was concentrated and purified by prep-HPLC or by silica gel column chromatography.

3-(1-(4-Bromophenyl)-3-(4-chlorophenyl)-1H-pyrazol-4-yl)-N-(methylsulfonyl)propanamide (1). **Method 3.** Yield: 19%. ¹H NMR (400 MHz, DMSO-*d*₆): δ 11.92–11.73 (m, 1H), 8.49–8.36 (m, 1H), 7.88–7.78 (m, 2H), 7.78–7.64 (m, 4H), 7.60–7.49 (m, 2H), 3.21 (s, 3H), 2.98–2.85 (m, 2H), 2.70–2.58 (m, 2H). ¹³C NMR (101 MHz, DMSO-*d*₆): δ 171.8, 149.5, 138.6, 132.7, 132.4 (2C), 131.8, 129.1 (2C), 128.7 (2C), 127.8, 120.1, 119.9 (2C), 118.4, 41.0, 35.7, 19.2. LC/MS (APCI⁺): calculated for C₁₉H₁₇BrClN₃O₃S, 480.99; observed *m/z* [M + H]⁺ 482.0, 483.9; HPLC purity: >99%.

3-(3-(4-Chlorophenyl)-1-phenyl-1H-pyrazol-4-yl)-N-(methylsulfonyl)propanamide (2). **Method 2.** Yield: 32%. ¹H NMR (400 MHz, DMSO-*d*₆): δ 12.09–11.57 (m, 1H), 8.45–8.34 (m, 1H), 7.89–7.81 (m, 2H), 7.81–7.71 (m, 2H), 7.62–7.46 (m, 4H), 7.37–7.29 (m, 1H), 3.18 (s, 3H), 3.00–2.86 (m, 2H), 2.64–2.57 (m, 2H). LC/MS (APCI⁺): calculated for C₁₉H₁₈ClN₃O₃S, 403.08; observed *m/z* [M + H]⁺ 404.1; HPLC purity: >99%.

3-(3-(4-Fluorophenyl)-1-(4-fluorophenyl)-1H-pyrazol-4-yl)-N-(methylsulfonyl)propanamide (3). **Method 1.** Yield: 14%. ¹H NMR (300 MHz, DMSO-*d*₆): δ 11.72 (s, 1H), 8.36 (s, 1H), 7.91–7.84 (m, 2H), 7.78–7.71 (m, 2H), 7.59–7.52 (m, 2H), 7.37 (t, *J* = 8.8 Hz, 2H), 3.21 (s, 3H), 2.93 (t, *J* = 7.5 Hz, 2H), 2.63 (t, *J* = 7.5 Hz, 2H). LC/MS (ESI⁺): calculated for C₁₉H₁₇ClF₂N₃O₃S, 421.07; observed *m/z* [M + H]⁺ 422.1; HPLC purity: 97%.

3-(1-(3-Bromophenyl)-3-(4-chlorophenyl)-1H-pyrazol-4-yl)-N-(methylsulfonyl)propanamide (4). **Method 1.** Yield: 20%. ¹H NMR (300 MHz, DMSO-*d*₆): δ 11.72 (s, 1H), 8.48 (s, 1H), 8.09 (t, *J* = 1.9 Hz, 1H), 7.88 (dt, *J* = 7.2, 2.0 Hz, 1H), 7.81–7.73 (m, 2H), 7.60–7.43 (m, 4H), 3.21 (s, 3H), 2.93 (t, *J* = 7.5 Hz, 2H), 2.64 (t, *J* = 7.5 Hz, 2H). LC/MS (APCI⁺): calculated for C₁₉H₁₇BrClN₃O₃S, 480.99; observed *m/z* [M + H]⁺ 481.9, 483.9; HPLC purity: 97%.

3-(1-(2-Bromophenyl)-3-(4-chlorophenyl)-1H-pyrazol-4-yl)-N-(methylsulfonyl)propanamide (5). **Method 2.** Yield: 31%. ¹H NMR (400 MHz, Chloroform-*d*): δ 7.74–7.65 (m, 5H), 7.60–7.58 (m, 3H), 7.45–7.43 (m, 1H), 3.27–3.25 (m, 3H), 3.13–3.07 (m, 2H), 2.64–2.58 (m, 2H). LC/MS (APCI⁺): calculated for C₁₉H₁₇BrClN₃O₃S, 480.99; observed *m/z* [M + H]⁺ 482.0; 484.0; HPLC purity: >99%.

3-(3-(4-Chlorophenyl)-1-(pyridin-4-yl)-1H-pyrazol-4-yl)-N-(methylsulfonyl)propanamide (6). **Method 2.** Yield: 23%. ¹H NMR (400 MHz, DMSO-*d*₆): δ 8.67–8.62 (m, 2H), 8.62–8.57 (m, 1H), 8.22–8.14 (m, 1H), 7.89–7.85 (m, 2H), 7.81–7.76 (m, 2H), 7.60–7.55 (m, 2H), 3.00–2.97 (m, 3H), 2.90–2.86 (m, 2H); ¹H NMR (400 MHz, DMSO-*d*₆ + D₂O): δ 8.64–8.56 (m, 2H), 8.51–8.45 (m, 1H), 8.29–8.12 (m, 1H), 7.86–7.79 (m, 2H), 7.78–7.68 (m, 2H), 7.58–7.50 (m, 2H), 3.03 (s, 3H), 2.90–2.81 (m, 2H). LC/MS (APCI⁺): calculated for C₁₈H₁₇ClN₄O₃S, 404.07; observed *m/z* [M + H]⁺ 405.0; HPLC purity: 98%.

3-(3-(4-Chlorophenyl)-1-cyclohexyl-1H-pyrazol-4-yl)-N-(methylsulfonyl)propanamide (7). Method 2. Yield: 37%. ¹H NMR (400 MHz, Chloroform-*d*): δ 7.74 (s, 1H), 7.57–7.55 (m, 2H), 7.42–7.40 (m, 2H), 7.35 (s, 1H), 4.14–4.10 (m, 1H), 3.26 (s, 3H), 3.04–3.00 (t, *J* = 7.2 Hz, 2H), 2.54–2.51 (t, *J* = 7.2 Hz, 2H), 2.20–2.17 (m, 2H), 1.94–1.91 (m, 2H), 1.77–1.71 (m, 3H), 1.46–1.26 (m, 3H). LC/MS (APCI⁺): calculated for C₁₉H₂₄ClN₃O₃S, 409.12; observed *m/z* [M + H]⁺ 410.0; HPLC purity: 96%.

3-(1,3-Bis(4-chlorophenyl)-1H-pyrazol-5-yl)-N-(methylsulfonyl)propanamide (8). Method 1. Yield: 52%. ¹H NMR (300 MHz, methanol-*d*₄): δ 8.14 (s, 1H), 7.84–7.75 (m, 2H), 7.76–7.66 (m, 2H), 7.54–7.46 (m, 4H), 3.21 (s, 3H), 3.10–2.98 (m, 2H), 2.64 (t, *J* = 7.4 Hz, 2H). ¹³C NMR (151 MHz, methanol-*d*₄): δ 174.0, 151.9, 140.0, 135.1, 133.3, 132.9, 130.6 (2C), 130.5 (2C), 129.8 (2C), 129.0 (2C), 121.3 (2C), 41.4, 37.4, 20.4. LC/MS (ESI⁺): calculated for C₁₉H₁₇Cl₂N₃O₃S, 437.04; observed *m/z* [M + H]⁺ 438.1; HPLC purity: >99%.

3-(3-(4-Chlorophenyl)-1-(4-(trifluoromethyl)phenyl)-1H-pyrazol-4-yl)-N-(methylsulfonyl)propanamide (9). Method 3. Yield: 11%. ¹H NMR (400 MHz, chloroform-*d*): 7.92 (s, 1H), 7.85–7.83 (d, *J* = 8.4 Hz, 2H), 7.70–7.63 (m, 4H), 7.44–7.42 (d, *J* = 8.8 Hz, 2H), 3.21 (s, 3H), 3.05–3.03 (m, 2H), 2.61–2.57 (m, 2H). LC/MS (ESI⁺): calculated for C₂₀H₁₇ClF₃N₃O₃S, 471.06; observed *m/z* [M + H]⁺ 472.1, 474.1; HPLC purity: 98%.

3-(3-(4-Chlorophenyl)-1-(6-(trifluoromethyl)pyridin-3-yl)-1H-pyrazol-4-yl)-N-(methylsulfonyl)propanamide (10). Method 1. Yield: 22%. ¹H NMR (400 MHz, Methanol-*d*₄): δ 9.22 (d, *J* = 2.5 Hz, 1H), 8.42 (ddd, *J* = 8.6, 2.6, 0.8 Hz, 1H), 8.34 (d, *J* = 0.9 Hz, 1H), 7.92 (dd, *J* = 8.6, 0.7 Hz, 1H), 7.80–7.62 (m, 2H), 7.56–7.43 (m, 2H), 3.21 (s, 3H), 3.11–2.97 (m, 2H), 2.66 (t, *J* = 7.3 Hz, 2H). ¹³C NMR (151 MHz, methanol-*d*₄): δ 174.2, 153.4, 145.6 (q, *J* = 35.4 Hz), 141.1, 139.7, 135.5, 132.8, 130.6 (2C), 129.9, 129.4, 127.7, 125.7, 123.9, 122.7 (d, *J* = 10.1 Hz), 122.1, 41.4, 37.3, 20.5. LC/MS (APCI⁺): calculated for C₁₉H₁₆ClF₃N₄O₃S, 472.06; observed *m/z* [M + H]⁺ 473.0; HPLC purity: >99%.

3-(3-(4-Chlorophenyl)-1-(4-cyanophenyl)-1H-pyrazol-4-yl)-N-(methylsulfonyl)propanamide (11). Method 3. Yield: 33%. ¹H NMR (400 MHz, chloroform-*d*): δ 7.96 (s, 1H), 7.89–7.87 (m, 2H), 7.78–7.76 (m, 2H), 7.67–7.65 (m, 2H), 7.49–7.47 (m, 2H), 3.31 (s, 3H), 3.14–3.10 (m, 2H), 2.63–2.59 (m, 2H). LC/MS (APCI⁺): calculated for C₂₀H₁₇ClN₄O₃S, 428.07; observed *m/z* [M + H]⁺ 429.1; HPLC purity: >99%.

3-(3-(4-Chlorophenyl)-1-(4-(methylsulfinyl)phenyl)-1H-pyrazol-4-yl)-N-(methylsulfonyl)propanamide (12). Step 1. 3-(3-(4-Chlorophenyl)-1-(4-(methylthio)phenyl)-1H-pyrazol-4-yl)-N-(methylsulfonyl)propanamide from acid 63l following sulfonamide coupling method 2 (Scheme S1). Yield: 40 mg (31%). ¹H NMR (400 MHz, chloroform-*d*): 7.83 (s, 1H), 7.67–7.65 (m, 4H), 7.47–7.46 (m, 3H), 7.45–7.34 (m, 2H), 3.28 (s, 3H), 3.12–3.08 (m, 2H), 2.62–2.58 (m, 2H), 2.54 (s, 3H). LC/MS (APCI⁺): calculated for C₂₀H₂₀ClN₃O₃S₂, 449.06; observed *m/z* [M + H]⁺ 450.0; HPLC purity: 95%.

Step 2. To a solution of 3-(3-(4-chlorophenyl)-1-(4-(methylthio)phenyl)-1H-pyrazol-4-yl)-N-(methylsulfonyl)propanamide (35 mg, 77.78 μ mol) in MeOH (200 μ L) and THF (200 μ L) was added NaIO₄ (17 mg, 81.67 μ mol, 5 μ L). The mixture was stirred at 20 °C for 15 h. The reaction mixture was diluted with aqueous Na₂SO₃ (5 mL) and extracted with EtOAc (10 mL \times 2). The combined organic layers were dried over Na₂SO₄ and concentrated. The residue was purified by prep-HPLC (column: Phenomenex Synergi C18 150 \times 25 \times 10 μ m; mobile phase: [water (0.225%FA)-ACN]; B %: 35–65%, 12 min) to give 3-(3-(4-chlorophenyl)-1-(4-(methylsulfinyl)phenyl)-1H-pyrazol-4-yl)-N-(methylsulfonyl)propanamide (12). Yield: 21 mg (58%). ¹H NMR (400 MHz, chloroform-*d*): δ 7.90–7.88 (m, 3H), 7.73–7.66 (m, 4H), 7.48–7.46 (m, 2H), 3.30 (s, 3H), 3.13–3.09 (m, 2H), 2.78 (s, 3H), 2.67–2.64 (m, 2H). LC/MS (APCI⁺): calculated for C₂₀H₂₀ClN₃O₄S₂, 465.06; observed *m/z* [M + H]⁺ 466.0, 468.0; HPLC purity: >99%.

3-(1-(4-Bromophenyl)-3-phenyl-1H-pyrazol-4-yl)-N-(methylsulfonyl)propanamide (13). Method 2. Yield: 29%. ¹H NMR

(400 MHz, chloroform-*d*): δ 7.76 (s, 1H), 7.62–7.60 (m, 2H), 7.57–7.38 (m, 7H), 3.18 (s, 3H), 3.06–3.02 (t, *J* = 7.2 Hz, 2H), 2.51–2.48 (t, *J* = 7.2 Hz, 2H). LC/MS (APCI⁺): calculated for C₁₉H₁₈BrN₃O₃S, 447.03; observed *m/z* [M + H]⁺ 448.0; HPLC purity: 99%.

3-(1-(4-Bromophenyl)-3-(3-chlorophenyl)-1H-pyrazol-4-yl)-N-(methylsulfonyl)propanamide (14). Method 2. Yield: 10%. ¹H NMR (400 MHz, chloroform-*d*): δ 7.83 (s, 1H), 7.70 (s, 1H), 7.64–7.53 (m, 5H), 7.43–7.34 (m, 2H), 3.26 (s, 3H), 3.07 (t, *J* = 7.2 Hz, 2H), 2.58 (t, *J* = 7.2 Hz, 2H). LC/MS (APCI⁺): calculated for C₁₉H₁₇BrClN₃O₃S, 480.99; observed *m/z* [M + H]⁺ 482.0, 484.0; HPLC purity: >99%.

3-(3-(2-Chlorophenyl)-1-(4-chlorophenyl)-1H-pyrazol-4-yl)-N-(methylsulfonyl)propanamide (15). Method 1. Yield: 9%. ¹H NMR (300 MHz, methanol-*d*₄): δ 8.13 (d, *J* = 0.8 Hz, 1H), 7.73 (d, *J* = 8.9 Hz, 2H), 7.57–7.52 (m, 1H), 7.50–7.36 (m, 5H), 3.17 (s, 3H), 2.76 (t, *J* = 7.4 Hz, 2H), 2.58–2.43 (m, 2H). LC/MS (APCI⁺): calculated for C₁₉H₁₇Cl₂N₃O₃S, 437.04; observed *m/z* [M + H]⁺ 437.9, 439.9 (chlorine isotopic pattern); HPLC purity: >99%.

3-(1-(4-Bromophenyl)-3-(pyridin-4-yl)-1H-pyrazol-4-yl)-N-(methylsulfonyl)propanamide (16). Method 3. Yield: 19%. ¹H NMR (400 MHz, DMSO-*d*₆): δ 8.74–8.63 (m, 2H), 8.51–8.47 (m, 1H), 7.88–7.83 (m, 2H), 7.74 (s, 4H), 3.10–3.07 (s, 3H), 2.99–2.93 (m, 2H), 2.59–2.55 (m, 2H). ¹³C NMR (151 MHz, DMSO-*d*₆): δ 172.3, 150.1 (2C), 147.9, 140.2, 138.5, 132.4 (2C), 128.4, 121.6 (2C), 121.2, 120.2 (2C), 118.8, 40.9, 36.1, 19.4. LC/MS (APCI⁺): calculated for C₁₈H₁₇BrN₄O₃S, 448.02; observed *m/z* [M + H]⁺ 449.0; HPLC purity: 97%.

3-(1-(4-Bromophenyl)-3-(pyridin-3-yl)-1H-pyrazol-4-yl)-N-(methylsulfonyl)propanamide (17). Method 3. Yield: 6%. ¹H NMR (400 MHz, chloroform-*d*): δ 8.79 (s, 1H), 8.45–8.44 (d, *J* = 4.4 Hz, 1H), 8.04–8.02 (d, *J* = 7.6 Hz, 1H), 7.83 (s, 1H), 7.56–7.50 (m, 4H), 7.31–7.30 (m, 1H), 3.19 (s, 3H), 3.01 (m, 2H), 2.59–2.56 (m, 2H). ¹³C NMR (151 MHz, chloroform-*d*): δ 171.8, 147.7, 147.1, 146.6, 138.7, 137.0, 132.7, 132.6, 130.4, 128.1, 127.0, 124.6, 120.5, 120.2, 119.9, 41.7, 37.3, 19.8. LC/MS (APCI⁺): calculated for C₁₈H₁₇BrN₄O₃S, 448.02; observed *m/z* [M + H]⁺ 449.0, 451.0 (1:1) bromine isotopic pattern; HPLC purity: >99%.

3-(1-(4-Bromophenyl)-3-(pyrazin-2-yl)-1H-pyrazol-4-yl)-N-(methylsulfonyl)propanamide (18). Method 2. Yield: 12%. ¹H NMR (400 MHz, chloroform-*d*): δ 9.44 (s, 1H), 8.67 (br s, 1H), 8.58 (s, 1H), 7.91 (s, 1H), 7.63 (q, *J* = 9.0 Hz, 4H), 3.28–3.19 (m, 5H), 2.79 (t, *J* = 7.1 Hz, 2H). LC/MS (APCI⁺): calculated for C₁₇H₁₆BrN₅O₃S, 449.02; observed *m/z* [M + H]⁺ 449.8, 451.9 (1:1) bromine isotopic pattern; HPLC purity: 91%.

3-(1-(4-Bromophenyl)-3-cyclohexyl-1H-pyrazol-4-yl)-N-(methylsulfonyl)propanamide (19). Method 2. Yield: 40%. ¹H NMR (400 MHz, chloroform-*d*): δ 8.17 (s, 1H), 7.65 (s, 1H), 7.52 (s, 4H), 3.30 (s, 3H), 2.93–2.82 (m, 2H), 2.60 (s, 3H), 1.88 (br s, 4H), 1.80–1.62 (m, 3H), 1.35 (s, 3H). LC/MS (APCI⁺): calculated for C₁₉H₂₄BrN₃O₃S, 453.07; observed *m/z* [M + H]⁺ 454.0; HPLC purity: >99%.

3-(1-(4-Bromophenyl)-3-(tetrahydro-2H-pyran-4-yl)-1H-pyrazol-4-yl)-N-(methylsulfonyl)propanamide (20). Method 2. Yield: 13%. ¹H NMR (400 MHz, DMSO-*d*₆): δ 8.18 (s, 1H), 7.71–7.62 (m, 4H), 3.94–3.92 (m, 2H), 3.46–3.45 (m, 2H), 3.43–3.26 (m, 2H), 3.07 (s, 3H), 2.70–2.69 (m, 1H), 2.67–2.66 (m, 3H), 1.77–1.73 (m, 4H). ¹³C NMR (151 MHz, DMSO-*d*₆): δ 172.7, 155.6, 138.9, 132.2 (2C), 126.2, 119.7, 119.4 (2C), 117.4, 67.1 (2C), 40.9, 36.9, 32.6, 31.9 (2C), 18.4. LC/MS (APCI⁺): calculated for C₁₈H₂₂BrN₃O₄S, 455.05; observed *m/z* [M + H]⁺ 456.0; HPLC purity: 98%.

3-(1-(4-Bromophenyl)-3-(piperidin-4-yl)-1H-pyrazol-4-yl)-N-(methylsulfonyl)propanamide (21). Step 1. *Tert*-butyl 4-(1-(4-bromophenyl)-4-(3-(methylsulfonamido)-3-oxopropyl)-1H-pyrazol-3-yl)piperidine-1-carboxylate was obtained as a white solid. Yield: 60 mg (17%) from acid 67 h by sulfonamide coupling method 2 (Scheme S2). LC/MS (APCI⁺): calculated for C₂₃H₃₁BrN₄O₅S, 554.12; observed *m/z* [M + H-Boc]⁺ 455.0; HPLC purity: 83%.

Step 2. The mixture of *tert*-butyl 4-(1-(4-bromophenyl)-4-(3-(methylsulfonamido)-3-oxopropyl)-1H-pyrazol-3-yl)piperidine-1-carboxylate (55 mg, 99.01 μ mol) in TFA (100 μ L) and DCM (1 mL)

was stirred at 20 °C for 2 h. The reaction mixture was concentrated. The obtained residue was purified by prep-HPLC (column: Phenomenex Synergi C18 150 × 25 × 10 μm, mobile phase: [water (0.225%FA)-ACN]; B %: 5–35%, 12 min) to give 3-(1-(4-bromophenyl)-3-(piperidin-4-yl)-1H-pyrazol-4-yl)-N-(methylsulfonyl)propanamide (**21**) as a white solid. Yield: 27 mg (59%). ¹H NMR (400 MHz, DMSO-*d*₆): δ 8.22 (s, 1H), 7.71–7.62 (m, 4H), 3.36–3.33 (m, 3H), 3.06 (s, 3H), 2.77–2.63 (m, 2H), 2.49–2.27 (m, 2H), 2.01–1.91 (m, 4H). LC/MS (APCI⁺): calculated for C₁₈H₂₃BrN₄O₃S, 454.07; observed *m/z* [M + H]⁺ 455.0; HPLC purity: 99%.

3-(1-(4-Bromophenyl)-3-(1-formylpiperidin-4-yl)-1H-pyrazol-4-yl)-N-(methylsulfonyl)propanamide (**22**). Method 2. Yield: 32%. ¹H NMR (400 MHz, DMSO-*d*₆): δ 8.21 (s, 1H), 8.03 (s, 1H), 7.71–7.63 (m, 4H), 4.26–4.22 (m, 1H), 3.79–3.76 (m, 1H), 3.19 (s, 3H), 3.00–2.80 (m, 1H), 2.79–2.59 (m, 6H), 2.34–1.54 (m, 4H). LC/MS (APCI⁺): calculated for C₁₉H₂₃BrN₄O₄S, 482.06; observed *m/z* [M + H]⁺ 483.1; HPLC purity: >99%.

3-(1-(4-Bromophenyl)-3-(4-nitrophenyl)-1H-pyrazol-4-yl)-N-(methylsulfonyl)propanamide (**23**). Method 2. Yield: 71%. ¹H NMR (400 MHz, methanol-*d*₄): δ 8.38–8.30 (m, 2H), 8.22 (d, *J* = 6.3 Hz, 1H), 8.06–7.98 (m, 2H), 7.82–7.74 (m, 2H), 7.69–7.61 (m, 2H), 3.16 (s, 3H), 3.09 (t, *J* = 7.5 Hz, 2H), 2.65 (t, *J* = 7.5 Hz, 2H). LC/MS (ESI⁺): calculated for C₁₉H₁₇BrN₄O₅S, 492.01; observed *m/z* [M + H]⁺ 493.0, 495.0 (1:1) bromine isotopic pattern; HPLC purity: 93%.

3-(3-(4-Aminophenyl)-1-(4-bromophenyl)-1H-pyrazol-4-yl)-N-(methylsulfonyl)propanamide (**24**). To a mixture of 3-(1-(4-bromophenyl)-3-(4-nitrophenyl)-1H-pyrazol-4-yl)-N-(methylsulfonyl)propanamide (**23**) (100 mg, 0.203 mmol) and iron (53 mg, 0.953 mmol) in EtOH (2 mL) was added a saturated solution of NH₄Cl (1 mL) and heated to 80 °C for 18 h. The reaction mixture was cooled to 25 °C, and the organic layer was separated. The organic layer was dried over Na₂SO₄, and the solvent was evaporated under reduced pressure. The residue was purified by flash silica gel column using DCM: MeOH (0–5% gradient) as eluents to afford 3-(3-(4-aminophenyl)-1-(4-bromophenyl)-1H-pyrazol-4-yl)-N-(methylsulfonyl)propanamide (**24**) as a gray solid. Yield: 5 mg (5%). ¹H NMR (400 MHz, methanol-*d*₄): δ 8.19 (s, 1H), 7.90 (d, *J* = 8.5 Hz, 2H), 7.76 (d, *J* = 8.8 Hz, 2H), 7.66 (d, *J* = 8.8 Hz, 2H), 7.49 (d, *J* = 8.5 Hz, 2H), 3.23 (s, 3H), 3.06 (t, *J* = 7.4 Hz, 2H), 2.68 (t, *J* = 7.4 Hz, 2H). LC/MS (APCI⁺): calculated for C₁₉H₁₉BrN₄O₃S, 462.04; observed *m/z* [M + H]⁺ 463.1, 465.1 (1:1) bromine isotopic pattern; HPLC purity: 92%.

3-(3-Benzyl-1-(4-bromophenyl)-1H-pyrazol-4-yl)-N-(methylsulfonyl)propanamide (**25**). Method 3. Yield: 20%. ¹H NMR (400 MHz, chloroform-*d*): δ 7.71 (s, 1H), 7.58 (s, 4H), 7.36–7.32 (m, 5H), 4.09 (s, 2H), 3.21 (s, 3H), 2.74–2.71 (m, 2H), 2.06–2.02 (m, 2H). LC/MS (APCI⁺): calculated for C₂₀H₂₀BrN₃O₃S, 461.04; observed *m/z* [M + H]⁺ 462.0; HPLC purity: >99%.

3-(1-(4-Bromophenyl)-3-(4-chlorophenyl)-1H-pyrazol-4-yl)propanoic Acid (**26**). To a solution of (E)-3-(1-(4-bromophenyl)-3-(4-chlorophenyl)-1H-pyrazol-4-yl)acrylic acid (**62a**) (1.66 g, 4.11 mmol) in MeOH (150 mL) was added NH₂NH₂·H₂O (16.47 g, 328.99 mmol, 16 mL), and the mixture was heated to 80 °C for 48 h (Scheme S1). The mixture was cooled to room temperature, diluted with ice water (100 mL) and adjusted to pH = 3 with 1 M HCl. The aqueous layer was extracted with DCM (50 mL × 3). The organic layer was washed with brine (50 mL), dried over anhydrous Na₂SO₄, and concentrated. To the residue was added petroleum ether (20 mL) slowly. The mixture was concentrated slowly to give some solid. The solid collected to give 3-(1-(4-bromophenyl)-3-(4-chlorophenyl)-1H-pyrazol-4-yl)propanoic acid (**26**) as a yellow solid. Yield: 1.80 g (99%). ¹H NMR (400 MHz, chloroform-*d*): δ 7.85–7.75 (m, 1H), 7.59 (d, *J* = 7.8 Hz, 6H), 7.48–7.38 (m, 2H), 3.02 (m, 2H), 2.67 (m, 2H). LC/MS (APCI⁺): calculated for C₁₈H₁₄BrClN₃O₃, 403.99; observed *m/z* [M + H]⁺ 404.9, 407.0; HPLC purity: 92%.

3-(1-(4-Bromophenyl)-3-(4-chlorophenyl)-1H-pyrazol-4-yl)-N-methylpropanamide (**27**). Method 3. To a solution of MeNH₂/THF (2 M, 5 mL) was added the solution of 3-(1-(4-bromophenyl)-3-(4-

chlorophenyl)-1H-pyrazol-4-yl)propanoyl chloride (**68**) (220 mg, 518.72 μmol) in DCM (2 mL) at –50 °C (Scheme S3). The mixture was stirred at –30 °C for ~3 h. The mixture was washed with water (5 mL) and concentrated. The residue was purified by prep-HPLC to give 3-(1-(4-bromophenyl)-3-(4-chlorophenyl)-1H-pyrazol-4-yl)-N-methylpropanamide (**27**) as a light-yellow solid. Yield: 60 mg (27%). ¹H NMR (300 MHz, DMSO-*d*₆): δ 8.42 (s, 1H), 7.85–7.81 (m, 2H), 7.77–7.75 (m, 2H), 7.72–7.70 (m, 2H), 7.56–7.54 (m, 2H), 2.89 (t, *J* = 7.6 Hz, 2H), 2.56 (d, *J* = 8.4 Hz, 3H), 2.43 (t, *J* = 7.6 Hz, 2H). LC/MS (APCI⁺): calculated for C₁₉H₁₇BrClN₃O, 417.02; observed *m/z* [M + H]⁺ 418.0, 420.0; HPLC purity: 98%.

3-(1-(4-Bromophenyl)-3-(4-chlorophenyl)-1H-pyrazol-4-yl)-N-methyl-N-(methylsulfonyl)propanamide (**28**). To a solution of N-methylmethanesulfonamide (116 mg, 1.06 mmol) in THF (5.00 mL) was added NaH 60% dispersion (45 mg, 1.13 mmol) at 0–10 °C. After stirring at 15 °C for 1 h, a solution of 3-(1-(4-bromophenyl)-3-(4-chlorophenyl)-1H-pyrazol-4-yl)propanoyl chloride (**68**) (300 mg, 707.35 μmol) in DCM (3.00 mL) was added at –10 °C via a syringe. The mixture was stirred at 15 °C for another 2 h. The mixture was washed with brine (5 mL) and concentrated. The residue was purified by prep-HPLC to give 3-(1-(4-bromophenyl)-3-(4-chlorophenyl)-1H-pyrazol-4-yl)-N-methyl-N-(methylsulfonyl)propanamide (**28**). Yield: 65 mg (17%). ¹H NMR (300 MHz, methanol-*d*₄): δ 8.25–8.17 (m, 1H), 7.80–7.71 (m, 4H), 7.69–7.61 (m, 2H), 7.54–7.46 (m, 2H), 3.27 (s, 6H), 3.11–2.98 (m, 4H). LC/MS (APCI⁺): calculated for C₂₀H₁₉BrClN₃O₃S, 495.00; Observed *m/z* [M + H]⁺ 496.0, 498.0; HPLC purity: 98%.

N-(3-(1-(4-Bromophenyl)-3-(4-chlorophenyl)-1H-pyrazol-4-yl)propyl)methanesulfonamide (**29**). To a solution of 3-(1-(4-bromophenyl)-3-(4-chlorophenyl)-1H-pyrazol-4-yl)propan-1-amine (**72**) (90 mg, 230.36 μmol) in DCM (3 mL) were added Et₃N (93 mg, 921.44 μmol, 128 μL) and MsCl (36 μL) at 0–10 °C (Scheme S3). The mixture was stirred at 10 °C for 1 h. The mixture was quenched with water (2 mL) and extracted with DCM (5 mL × 2). The organic phase was concentrated and purified by reverse-phase HPLC to give N-(3-(1-(4-bromophenyl)-3-(4-chlorophenyl)-1H-pyrazol-4-yl)propyl)methanesulfonamide (**29**) as a white solid. Yield: 68 mg (63%). ¹H NMR (400 MHz, DMSO-*d*₆): δ 8.54–8.41 (m, 1H), 7.91–7.81 (m, 2H), 7.81–7.74 (m, 2H), 7.74–7.66 (m, 2H), 7.60–7.48 (m, 2H), 7.12–7.00 (m, 1H), 3.10–2.96 (m, 2H), 2.89 (s, 3H), 2.76–2.69 (m, 2H), 1.87–1.73 (m, 2H). LC/MS (APCI⁺): calculated for C₁₉H₁₉BrClN₃O₂S, 467.01; observed *m/z* [M + H]⁺ 468.0; HPLC purity: >99%.

N-((2-(1-(4-Bromophenyl)-3-(4-chlorophenyl)-1H-pyrazol-4-yl)ethyl)sulfonyl)acetamide (**30**). To the solution of 2-(1-(4-bromophenyl)-3-(4-chlorophenyl)-1H-pyrazol-4-yl)ethane-1-sulfonamide (**74**) (150 mg, 340.34 μmol) and Et₃N (69 mg, 680.68 μmol, 94 μL) in THF (4 mL) was added acetyl chloride (40 mg, 510.51 μmol, 36 μL) drop-wise in ice bath (Scheme S4). The mixture was stirred at 40 °C for 16 h. The mixture was concentrated and separated between water (3 mL) and EtOAc (3 mL). The organic phase was dried over anhydrous Na₂SO₄ and concentrated. The residue was purified by prep-HPLC (column: Phenomenex Synergi C18150 × 25 × 10 μm; mobile phase: [water (0.225%FA)-ACN]; B %: 57–87%, 10 min) and then purified again by prep-HPLC (column: Phenomenex Gemini 150 × 25 mm × 10 μm; mobile phase: [water (0.05% ammonia hydroxide v/v)-ACN]; B %: 22–52%, 10 min) to afford N-((2-(1-(4-bromophenyl)-3-(4-chlorophenyl)-1H-pyrazol-4-yl)ethyl)sulfonyl)acetamide (**30**) as a white solid. Yield: 29 mg (17%). ¹H NMR (400 MHz, DMSO-*d*₆): δ 8.58 (s, 1H), 7.88–7.83 (m, 3H), 7.74–7.70 (m, 4H), 7.54–7.51 (m, 2H), 3.60–3.56 (m, 2H), 3.06–3.03 (m, 2H), 1.87 (s, 3H). LC/MS (APCI⁺): calculated for C₁₉H₁₇BrClN₃O₃S, 480.99; observed *m/z* [M + H]⁺ 482.0; HPLC purity: >99%.

2-(1-(4-Bromophenyl)-3-(4-chlorophenyl)-1H-pyrazol-4-yl)-N-(methylsulfonyl)acetamide (**31**). Method 2. Yield: 11%. ¹H NMR (400 MHz, chloroform-*d*): δ 8.05 (s, 1H), 7.88 (s, 1H), 7.67–7.60 (m, 6H), 7.49–7.47 (d, *J* = 8.4 Hz, 2H), 3.81 (s, 2H), 3.15 (s, 3H). LC/MS (APCI⁺): calculated for C₁₈H₁₅BrClN₃O₃S, 466.97; observed *m/z* [M + H]⁺ 467.9, 470.0; HPLC purity: 99%.

4-(1-(4-Bromophenyl)-3-(4-chlorophenyl)-1H-pyrazol-4-yl)-N-(methylsulfonyl)butanamide (32). Method 2. Yield: 9%. ¹H NMR (300 MHz, methanol-*d*₄): δ 8.20 (s, 1H), 7.78–7.72 (m, 4H), 7.66–7.64 (m, 2H), 7.50–7.48 (m, 2H), 3.17 (s, 3H), 2.79–2.75 (t, *J* = 7.6 Hz, 2H), 2.39–2.36 (t, *J* = 7.2 Hz, 2H), 1.99–1.95 (t, *J* = 7.6 Hz, 2H). LC/MS (APCI⁺): calculated for C₂₀H₁₉BrClN₃O₃S, 495.00; observed *m/z* [M + H]⁺ 496.0; HPLC purity: 96%.

3-(1-(4-Bromophenyl)-3-(4-chlorophenyl)-1H-pyrazol-4-yl)-N-(ethylsulfonyl) Propanamide (33). Method 1. Yield: 23%. ¹H NMR (300 MHz, methanol-*d*₄): δ 8.14 (s, 1H), 7.73 (ddt, *J* = 7.5, 4.7, 2.4 Hz, 4H), 7.69–7.61 (m, 2H), 7.53–7.46 (m, 2H), 3.42–3.35 (m, 2H), 3.05 (t, *J* = 7.3 Hz, 2H), 2.66 (t, *J* = 7.3 Hz, 2H), 1.25 (t, *J* = 7.4 Hz, 3H). LC/MS (ESI⁺): calculated for C₂₀H₁₉BrClN₃O₃S, 495.00; observed *m/z* [M + H]⁺ 496.1; HPLC purity: 98%.

3-(1-(4-Bromophenyl)-3-(4-chlorophenyl)-1H-pyrazol-4-yl)-N-(cyclopropylsulfonyl) Propanamide (34). Method 1. Yield: 25 mg (10%). ¹H NMR (300 MHz, methanol-*d*₄): δ 8.15 (s, 1H), 7.80–7.67 (m, 4H), 7.68–7.62 (m, 2H), 7.54–7.46 (m, 2H), 3.05 (t, *J* = 7.3 Hz, 2H), 2.98–2.86 (m, 1H), 2.65 (t, *J* = 7.3 Hz, 2H), 1.26–1.13 (m, 2H), 1.08–0.98 (m, 2H). LC/MS (APCI⁺): calculated for C₂₁H₁₉BrClN₃O₃S, 507.00; observed *m/z* [M + H]⁺ 508.1; HPLC purity: >99%.

3-(1-(4-Chlorophenyl)-3-(pyridin-4-yl)-1H-pyrazol-4-yl)-N-(methylsulfonyl)propanamide (35). Method 1. Yield: 8%. ¹H NMR (300 MHz, methanol-*d*₄): δ 8.68–8.58 (m, 2H), 8.21 (s, 1H), 7.89–7.80 (m, 4H), 7.57–7.48 (m, 2H), 3.23 (s, 3H), 3.14 (t, *J* = 7.4 Hz, 2H), 2.71 (t, *J* = 7.3 Hz, 2H). LC/MS (ESI⁺): calculated for C₁₈H₁₇ClN₄O₃S, 404.07; observed *m/z* [M + H]⁺ 405.1; HPLC purity: >99%.

3-(1-(4-Chlorophenyl)-3-(pyridin-4-yl)-1H-pyrazol-4-yl)-2-methyl-N-(methylsulfonyl)propanamide (36). Method 1. Yield: 18%. ¹H NMR (300 MHz, methanol-*d*₄): δ 8.68–8.61 (m, 2H), 8.17 (s, 1H), 7.88–7.80 (m, 4H), 7.56–7.49 (m, 2H), 3.15 (s, 4H), 2.98–2.84 (m, 1H), 2.80–2.66 (m, 1H), 1.25 (d, *J* = 6.9 Hz, 3H). LC/MS (ESI⁺): calculated for C₁₉H₁₉ClN₄O₃S, 418.09; observed *m/z* [M + H]⁺ 419.1; HPLC purity: >99%.

3-(1-(4-Chlorophenyl)-3-(pyridin-4-yl)-1H-pyrazol-4-yl)-N-(methylsulfonyl)butanamide (37). Method 1. Yield: 21%. ¹H NMR (300 MHz, methanol-*d*₄): δ 8.62 (d, *J* = 5.0 Hz, 2H), 8.28 (s, 1H), 7.94–7.76 (m, 4H), 7.51 (d, *J* = 8.9 Hz, 2H), 3.64 (q, *J* = 7.2 Hz, 1H), 3.10 (s, 3H), 2.75–2.54 (m, 2H), 1.35 (d, *J* = 7.2 Hz, 3H). LC/MS (ESI⁺): calculated for C₁₉H₁₉ClN₄O₃S, 418.09; observed *m/z* [M + H]⁺ 419.1; HPLC purity: >99%.

(E)-3-(1-(4-Chlorophenyl)-3-(pyridin-4-yl)-1H-pyrazol-4-yl)-N-(methylsulfonyl)acrylamide (38). Method 1. Isolated as hydrochloride salt. Yield: 21%. ¹H NMR (300 MHz, DMSO-*d*₆): δ 9.24 (s, 1H), 8.94 (d, *J* = 5.6 Hz, 2H), 8.10 (d, *J* = 5.7 Hz, 2H), 8.04–8.00 (m, 2H), 7.76–7.65 (m, 3H), 6.57 (d, *J* = 15.8 Hz, 1H), 3.32 (s, 3H). ¹³C NMR (101 MHz, DMSO-*d*₆): δ 164.4, 147.5, 145.5, 144.3 (2C), 137.4, 132.5, 132.1, 130.5, 129.7 (2C), 124.6 (2C), 120.9 (2C), 119.1, 118.6, 41.3. LC/MS (ESI⁺): calculated for C₁₈H₁₅ClN₄O₃S, 402.06; observed *m/z* [M + H]⁺ 403.0, 404.9; HPLC purity: 98%.

(E)-3-(1-(4-Bromophenyl)-3-(pyridin-4-yl)-1H-pyrazol-4-yl)-N-(methylsulfonyl)acrylamide (39). Method 1. Yield: 10%. ¹H NMR (300 MHz, methanol-*d*₄): δ 9.02–8.90 (m, 3H), 8.49–8.43 (m, 2H), 7.97–7.87 (m, 3H), 7.81–7.71 (m, 2H), 6.61 (d, *J* = 15.5 Hz, 1H), 3.34 (s, 3H). LC/MS (ESI⁺): calculated for C₁₈H₁₇BrN₄O₃S, 448.02; observed *m/z* [M + H]⁺ 448.8; HPLC purity: 99%.

2-(1-(4-Chlorophenyl)-3-(pyridin-4-yl)-1H-pyrazol-4-yl)-N-(methylsulfonyl)cyclopropane-1-carboxamide (40). Method 1. Yield: 39%. ¹H NMR (300 MHz, methanol-*d*₄): δ 8.91–8.83 (m, 2H), 8.60–8.52 (m, 2H), 8.41 (s, 1H), 7.96–7.89 (m, 2H), 7.62–7.55 (m, 2H), 3.35 (s, 3H), 2.78–2.68 (m, 1H), 1.96 (dt, *J* = 8.8, 4.7 Hz, 1H), 1.80 (dt, *J* = 9.3, 4.7 Hz, 1H), 1.58 (ddd, *J* = 8.1, 6.5, 4.3 Hz, 1H). ¹³C NMR (151 MHz, methanol-*d*₄): δ 172.1, 161.4, 161.1, 147.5, 147.1, 146.5, 144.1, 143.8, 138.5, 132.4, 128.7, 123.7, 123.3, 122.9, 120.4, 40.2, 24.3, 17.5, 15.6. LC/MS (ESI⁺): C₁₉H₁₇ClN₄O₃S, 416.07; observed *m/z* [M + H]⁺ 417.1; HPLC purity: >99%.

2-(1-(4-Bromophenyl)-3-(pyridin-4-yl)-1H-pyrazol-4-yl)-N-(methylsulfonyl)cyclopropane-1-carboxamide (41). Method 1. Yield: 22%. ¹H NMR (600 MHz, methanol-*d*₄): δ 8.74 (d, *J* = 5.7

Hz, 2H), 8.33–8.26 (m, 3H), 7.83–7.75 (m, 2H), 7.70–7.62 (m, 2H), 3.29 (s, 4H), 2.63 (ddd, *J* = 8.9, 6.6, 4.7 Hz, 1H), 1.88 (dt, *J* = 8.2, 4.7 Hz, 1H), 1.73 (dt, *J* = 9.2, 4.7 Hz, 1H), 1.51 (ddd, *J* = 8.2, 6.6, 4.7 Hz, 1H). ¹³C NMR (151 MHz, methanol-*d*₄): δ 173.6, 163.1, 162.9, 162.6, 148.5, 148.1, 148.0, 145.9, 145.6, 139.9, 130.1, 125.0, 124.6, 121.8, 121.7, 41.6, 25.8, 19.0, 17.0. LC/MS (ESI⁺): calculated for C₁₉H₁₇BrN₄O₃S, 460.02; observed *m/z* [M + H]⁺ 460.9; HPLC purity: >98%.

3-(3-(4-Bromophenyl)-1-(4-chlorophenyl)-1H-pyrazol-5-yl)-N-(methylsulfonyl)propanamide (51). Method 2. Yield: 25%. ¹H NMR (400 MHz, chloroform-*d*): δ 8.00 (s, 1H), 7.72–7.70 (m, 2H), 7.56–7.45 (m, 6H), 6.53 (s, 1H), 3.30 (s, 3H), 3.11–3.07 (t, *J* = 7.2 Hz, 2H), 2.69–2.65 (t, *J* = 7.2 Hz, 2H). LC/MS (APCI⁺): calculated for C₁₉H₁₇BrClN₃O₃S, 480.99; observed *m/z* [M + H]⁺ 482.0; HPLC purity: 99%.

3-(3-(4-Chlorophenyl)-1-(4-fluorophenyl)-1H-pyrazol-5-yl)-N-(methylsulfonyl)propanamide (52). Method 2. Yield: 20%. ¹H NMR (300 MHz, methanol-*d*₄): δ 7.85–7.76 (m, 2H), 7.64–7.53 (m, 2H), 7.46–7.39 (m, 2H), 7.39–7.28 (m, 2H), 6.71 (s, 1H), 3.21 (s, 3H), 3.00 (t, *J* = 7.3 Hz, 2H), 2.71 (t, *J* = 7.3 Hz, 2H). LC/MS (ESI⁺): calculated for C₁₉H₁₇ClF₂N₃O₃S, 421.07; observed *m/z* [M + H]⁺ 422.1; HPLC purity: 96%.

3-(1-(4-Bromophenyl)-4-(4-chlorophenyl)-1H-pyrazol-3-yl)-N-(methylsulfonyl)propanamide (53). Method 2. Yield: 15%. ¹H NMR (400 MHz, chloroform-*d*): δ 10.70 (s, 1H), 8.00 (s, 1H), 7.64–7.45 (m, 4H), 7.43–7.41 (m, 2H), 7.34–7.32 (m, 2H), 3.32 (s, 3H), 3.19–3.16 (t, *J* = 6.4 Hz, 2H), 2.89–2.86 (t, *J* = 6.4 Hz, 2H). LC/MS (APCI⁺): calculated for C₁₉H₁₇BrClN₃O₃S, 480.99; observed *m/z* [M + H]⁺ 482.0; HPLC purity: 95%.

3-(3,5-Bis(4-chlorophenyl)-1H-pyrazol-1-yl)-N-(methylsulfonyl)propanamide (54). Method 1. Yield: 11%. ¹H NMR (300 MHz, Methanol-*d*₄): δ 7.89–7.79 (m, 2H), 7.60–7.49 (m, 4H), 7.45–7.36 (m, 2H), 6.73 (s, 1H), 4.45 (t, *J* = 6.5 Hz, 2H), 3.14 (s, 3H), 2.97 (t, *J* = 6.5 Hz, 2H). LC/MS (ESI⁺): calculated for C₁₉H₁₇Cl₂N₃O₃S, 437.04; observed *m/z* [M + H]⁺ 438.0; HPLC purity: >99%.

3-(5-(4-Bromophenyl)-1-(4-chlorophenyl)-1H-pyrazol-3-yl)-N-(methylsulfonyl)propanamide (55). Method 2. Yield: 34%. ¹H NMR (400 MHz, chloroform-*d*): δ 10.71 (s, 1H), 7.50–7.49 (m, 2H), 7.38–7.36 (m, 2H), 7.27–7.25 (m, 2H), 7.11–7.09 (m, 2H), 6.37 (s, 1H), 3.30 (s, 3H), 3.13–3.11 (t, *J* = 6.0 Hz, 2H), 2.88–2.84 (t, *J* = 6.0 Hz, 2H). LC/MS (APCI⁺): calculated for C₁₉H₁₇BrClN₃O₃S, 480.99; observed *m/z* [M + H]⁺ 482.0; HPLC purity: >99%.

3-(2,4-Bis(4-chlorophenyl)oxazol-5-yl)-N-(methylsulfonyl)propanamide (56). Method 3. Yield: 11%. ¹H NMR (400 MHz, methanol-*d*₄): δ 8.06 (d, *J* = 6.80 Hz, 2H), 7.76 (d, *J* = 6.80 Hz, 2H), 7.54 (d, *J* = 6.80 Hz, 2H), 7.49 (d, *J* = 6.80 Hz, 2H), 3.32 (t, *J* = 5.60 Hz, 2H), 3.22 (s, 3H), 2.85 (t, *J* = 7.20 Hz, 2H). LC/MS (APCI⁺): calculated for C₁₉H₁₆Cl₂N₂O₄S, 439.31; observed *m/z* [M + H]⁺ 441.0. HPLC purity: 96%.

3-(2,4-Bis(4-chlorophenyl)thiazol-5-yl)-N-(methylsulfonyl)propanamide (57). Yield: 20%. ¹H NMR (400 MHz, methanol-*d*₄): δ 7.98–7.90 (m, 2H), 7.73–7.62 (m, 2H), 7.55–7.45 (m, 4H), 3.29 (d, *J* = 7.2 Hz, 2H), 3.20 (s, 3H), 2.73 (t, *J* = 7.2 Hz, 2H). LC/MS (ESI⁺): calculated for C₁₉H₁₆Cl₂N₂O₃S, 454.00; observed *m/z* [M + H]⁺ 455.0. HPLC purity: >99%.

General Procedure for the Synthesis of Carbamate 45 and Ureas (42–44 and 58). To a solution of methanesulfonamide (1.5–2.5 equiv) in DCM or DMF was added diisopropylethylamine (DIPEA, 7.5 equiv) and CDI (0.5–2.5 equiv) at 0 °C. The resulting mixture was stirred at 25 °C for 16 h. Then, the appropriate amine or alcohol (1 equiv) dissolved in DCM or DMF (depending on the solubility) was added and heated at 45–90 °C for 24–48 h. Solvents were evaporated under reduced pressure. Crude product was purified by preparative HPLC or silica gel column chromatography.

N-(((3-(Pyridin-4-yl)-1-(6-(trifluoromethyl)pyridin-3-yl)-1H-pyrazol-4-yl)methyl)carbamoyl)methanesulfonamide (42). Yield: 31%. ¹H NMR (400 MHz, methanol-*d*₄): δ 9.35 (d, *J* = 2.36 Hz, 1H), 8.85 (d, *J* = 5.96 Hz, 2H), 8.66 (s, 1H), 8.56 (dd, *J* = 2.36, 8.42 Hz, 1H), 8.37 (d, *J* = 6.48 Hz, 2H), 8.02 (d, *J* = 8.60 Hz, 1H), 4.67 (s, 2H), 3.25 (s, 3H). LC/MS (APCI⁺): calculated for C₁₇H₁₅F₃N₆O₃S, 440.40; observed *m/z* [M + H]⁺ 441.1.

N-(((1-(4-Chlorophenyl)-3-(pyridin-4-yl)-1*H*-pyrazol-4-yl)methyl)carbamoyl)methanesulfonamide (**43**). Yield: 19%. ¹H NMR (400 MHz, methanol-*d*₄): δ 8.88 (d, *J* = 5.44 Hz, 2H), 8.53 (d, *J* = 5.20 Hz, 2H), 8.49 (s, 1H), 7.93 (d, *J* = 7.72 Hz, 2H), 7.58 (d, *J* = 7.72 Hz, 2H), 4.68 (s, 2H), 3.26 (s, 3H). ¹³C NMR (151 MHz, methanol-*d*₄): δ 154.5, 149.8 (2C), 148.9, 143.7, 139.7, 133.7, 130.9, 130.7, 123.9, 123.7, 121.7, 121.5, 121.2, 120.6, 41.8, 35.5. LC/MS (APCI⁺): calculated for C₁₇H₁₆ClN₅O₃S, 405.86; observed *m/z* [M + H]⁺ 406.1; HPLC purity: 97%.

N-(((1,3-Bis(4-chlorophenyl)-1*H*-pyrazol-4-yl)methyl)carbamoyl)methanesulfonamide (**44**). Yield: 15%. ¹H NMR (300 MHz, DMSO-*d*₆): δ 10.00 (s, 1H), 8.51 (s, 1H), 7.94–7.88 (m, 2H), 7.80–7.74 (m, 2H), 7.63–7.53 (m, 4H), 6.85 (t, *J* = 5.4 Hz, 1H), 4.38 (d, *J* = 5.4 Hz, 2H), 3.22 (s, 3H). LC/MS (APCI⁺): calculated for C₁₈H₁₆Cl₂N₄O₃S, 438.03; observed *m/z* [M + H]⁺ 438.9, 440.9; HPLC purity: 96%.

(1-(4-Chlorophenyl)-3-(pyridin-4-yl)-1*H*-pyrazol-4-yl)methyl(methylsulfonyl)carbamate (**45**). Yield: 26%. ¹H NMR (400 MHz, DMSO-*d*₆): δ 11.81 (s, 1H), 8.81 (s, 1H), 8.71 (s, 2H), 7.95–7.98 (m, 2H), 7.79–7.80 (m, 2H), 7.62–7.64 (m, 2H), 5.29 (s, 2H), 3.24 (s, 3H). ¹³C NMR (101 MHz, DMSO-*d*₆): δ 152.4, 150.7, 150.5, 149.5, 139.7, 138.3, 132.0, 131.7, 130.1, 130.0 (2C), 122.3, 120.8, 120.5, 116.8, 58.4, 41.2. LC/MS (APCI⁺): calculated for C₁₇H₁₅ClN₄O₄S, 406.84; observed *m/z* [M + H]⁺ 407.1; HPLC purity: 98%.

N-(((5-(4-Bromophenyl)-2-(pyridin-4-yl)furan-3-yl)methyl)carbamoyl)methanesulfonamide (**58**). Yield: 29%. ¹H NMR (400 MHz, DMSO-*d*₆): δ 10.41 (s, 1H), 8.76 (d, *J* = 6.1 Hz, 2H), 8.00 (d, *J* = 6.1 Hz, 2H), 7.90–7.84 (m, 2H), 7.74–7.67 (m, 2H), 7.21 (s, 2H), 4.51 (d, *J* = 5.7 Hz, 2H), 3.24 (s, 3H). ¹³C NMR (151 MHz, DMSO-*d*₆): δ 158.2, 157.9, 153.5, 152.6, 146.0, 143.9, 140.1, 132.1 (2C), 129.9, 128.0, 126.3 (2C), 122.1, 119.9, 110.9, 41.4, 35.3. LC/MS (ESI⁺): calculated C₁₈H₁₆BrN₃O₄S, 449.00; observed *m/z* [M + H]⁺ 450.0, 452.0 (1:1) bromine isotopic pattern; HPLC purity: 96%.

Synthesis of Compounds with Heterocyclic Rings at C4–46–50. 5-(2-(1-(4-Bromophenyl)-3-(4-chlorophenyl)-1*H*-pyrazol-4-yl)ethyl)-1*H*-tetrazole (**46**). To a solution of 3-(1-(4-bromophenyl)-3-(4-chlorophenyl)-1*H*-pyrazol-4-yl)propanenitrile (**93**) (100 mg, 258.62 μmol) in isopropanol (1 mL) and water (500 μL) were added ZnBr₂ (58 mg, 258.62 μmol, 13 μL) and NaN₃ (50 mg, 775.86 μmol, 27 μL) (Scheme S8). The mixture was stirred at 120 °C for 15 h. The reaction mixture was diluted with water (10 mL) and extracted with EtOAc (10 mL × 2). The combined organic layers were dried over Na₂SO₄ and concentrated. The residue was purified by prep-HPLC (column: Phenomenex Synergi C18 150 × 30 mm × 4 μm; mobile phase: [water (0.225%FA)-ACN]; B %: 60–90%, 12 min) to afford 5-(2-(1-(4-bromophenyl)-3-(4-chlorophenyl)-1*H*-pyrazol-4-yl)ethyl)-1*H*-tetrazole (**46**) as a white solid. Yield: 21 mg (19%). ¹H NMR (300 MHz, DMSO-*d*₆): δ 8.52 (s, 1H), 7.85–7.83 (m, 2H), 7.77–7.70 (m, 4H), 7.56–7.54 (m, 2H), 3.22–3.18 (m, 2H), 3.12–3.10 (m, 2H). LC/MS (APCI⁺): calculated for C₁₈H₁₄BrClN₆O, 428.02; observed *m/z* [M + H]⁺ 429.0; HPLC purity: >99%.

3-(2-(1-(4-Bromophenyl)-3-(4-chlorophenyl)-1*H*-pyrazol-4-yl)ethyl)-1,2,4-oxadiazol-5(4*H*)-one (**47**). Step 1. To a mixture of 3-(1-(4-bromophenyl)-3-(4-chlorophenyl)-1*H*-pyrazol-4-yl)propanenitrile (**93**) (1.00 g, 2.59 mmol) and NH₂OH·H₂O (270 mg, 3.89 mmol) in water (5 mg, 259.00 μmol) and EtOH (10 mL) was added a solution of NaOMe (168 mg, 3.11 mmol) in MeOH (4 mL) (Scheme S8). The mixture was stirred at 90 °C for 6 h. The mixture was poured into water (10 mL) and stirred for 15 min. The solid was collected to afford (Z)-3-(1-(4-bromophenyl)-3-(4-chlorophenyl)-1*H*-pyrazol-4-yl)-*N'*-hydroxypropanimidamide (**94**) as a light-yellow solid. Yield: 1 g (crude). LC/MS (APCI⁺): calculated for C₁₈H₁₆BrClN₄O, 418.02; observed *m/z* [M + H]⁺ 419.0; HPLC purity: 69%.

Step 2. To a solution of (Z)-3-(1-(4-bromophenyl)-3-(4-chlorophenyl)-1*H*-pyrazol-4-yl)-*N'*-hydroxypropanimidamide (**94**) (250 mg, 411.01 μmol) in DMF (800 μL) and EtOH (2 mL) was added NaOMe (4 M, 206 μL). The mixture was stirred at 15 °C for 0.5 h, and diethylcarbonate (304 mg, 2.57 mmol, 310 μL) was added. The mixture was stirred at 80 °C for another 16 h. The mixture was

concentrated and diluted with water (5 mL). The aqueous phase was adjusted to pH = 7 with 1 N HCl and extracted with EtOAc (5 mL × 3). The organic phase was concentrated and purified by prep-HPLC (column: Phenomenex Synergi C18 150 × 25 × 10 μm; mobile phase: [water (0.225%FA)-ACN]; B %: 65–95%, 11 min) to afford 3-(2-(1-(4-bromophenyl)-3-(4-chlorophenyl)-1*H*-pyrazol-4-yl)ethyl)-1,2,4-oxadiazol-5(4*H*)-one (**47**) as a white solid. Yield: 58 mg (32%). ¹H NMR (400 MHz, chloroform-*d*): δ 9.41 (s, 1H), 7.86 (s, 1H), 7.66–7.54 (m, 6H), 7.47–7.40 (m, 2H), 3.17–3.02 (m, 2H), 2.88–2.77 (m, 2H). LC/MS (APCI⁺): calculated for C₁₉H₁₄BrClN₄O₂, 444.00; observed *m/z* [M + H]⁺ 445.0; HPLC purity: >99%.

5-((1,3-Bis(4-chlorophenyl)-1*H*-pyrazol-4-yl)methyl)pyrimidine-2,4,6(1*H*,3*H*,5*H*)-trione (**48**). To a solution of 1,3-bis(4-chlorophenyl)-1*H*-pyrazole-4-carbaldehyde (61 h) (0.150 g, 0.473 mmol) and pyrimidine-2,4,6(1*H*,3*H*,5*H*)-trione (0.064 g, 0.500 mmol) was added a mixture of EtOH (10 mL) and DMF (10 mL) (Scheme S9). The reaction mixture was heated in a pressure tube to 80 °C for 16 h. The resulting suspension was cooled to 25 °C, NaBH₄ (0.038 g, 1.004 mmol) was added, and the resulting mixture was stirred for 1 h at 25 °C to yield a clear orange solution. The solvents were evaporated *in vacuo* to afford a residue. To the obtained residue were added water (80 mL) and some NaCl and hexane (70 mL) and EtOAc (10 mL), and the resulting suspension was acidified with HCl to pH = 2 and stirred for 1 h. The resulting precipitate was filtered off, yielding a white solid. The water layer was reextracted with EtOAc (80 mL × 2), and the combined organic phases were dried over Na₂SO₄, evaporated, and purified by SiO₂ flash chromatography [CH₂Cl₂/iPrOH 95/5 to 90/10] yielding 5-((1,3-bis(4-chlorophenyl)-1*H*-pyrazol-4-yl)methyl)-5-hydroxypyrimidine-2,4,6(1*H*,3*H*,5*H*)-trione (0.027 g, 0.059 mmol, 12%) as a slightly yellowish solid (byproduct). The white precipitate showed broad signals in NMR [due to B(OH)₃ contamination] and was therefore dissolved in MeOH (80 mL) and HCl conc (1 mL), and the solvent was evaporated. This procedure was repeated to give 5-((1,3-bis(4-chlorophenyl)-1*H*-pyrazol-4-yl)methyl)pyrimidine-2,4,6(1*H*,3*H*,5*H*)-trione (**48**) as a yellow solid. Yield: 162 mg (78%). ¹H NMR (300 MHz, DMSO-*d*₆): δ 11.77 (s, 2H), 8.18 (s, 1H), 7.86 (d, *J* = 8.8 Hz, 2H), 7.69 (d, *J* = 8.4 Hz, 2H), 7.57 (d, *J* = 8.8 Hz, 2H), 7.53 (d, *J* = 8.4 Hz, 2H), 3.66 (s, 2H), 3.39 (s, 1H). LC/MS (ESI⁺): calculated for C₂₀H₁₄Cl₂N₄O₃, 428.04; observed *m/z* [M + H]⁺ 429.1, 431.0; HPLC purity: 98%.

5-(2-(1-(4-Bromophenyl)-3-(4-chlorophenyl)-1*H*-pyrazol-4-yl)ethyl)-1,3,4-oxadiazol-2(3*H*)-one (**49**). Step 1. The reaction mixture of 3-(1-(4-bromophenyl)-3-(4-chlorophenyl)-1*H*-pyrazol-4-yl)propanoic acid (**26**) (500 mg, 1.23 mmol), Et₃N (36 mg, 356.70 μmol, 49 μL), and NH₂NH₂·H₂O (157 mg, 3.08 mmol, 153 μL) in toluene was stirred at 130 °C for 3 h (Scheme S8). The mixture was separated between water (3 mL) and EtOAc (3 mL). The aqueous phase was extracted with EtOAc (3 mL × 2). The combined organic phase was washed with brine (5 mL), dried with anhydrous Na₂SO₄, filtered, and concentrated to afford crude 3-(1-(4-bromophenyl)-3-(4-chlorophenyl)-1*H*-pyrazol-4-yl)propanehydrazide (**95**) as a yellow solid. Yield: 250 mg (48%). LC/MS (APCI⁺): calculated for C₁₈H₁₆BrClN₄O, 418.02; observed *m/z* [M + H]⁺ 419.0; HPLC purity: 67%.

Step 2. To the solution of 3-(1-(4-bromophenyl)-3-(4-chlorophenyl)-1*H*-pyrazol-4-yl)propanehydrazide (**95**) (250 mg, 595.66 μmol) in THF (5 mL) was added CDI (145 mg, 893.49 μmol). The mixture was stirred at 60 °C for 4 h under a nitrogen atmosphere. The mixture was poured into water (5 mL) and extracted with EtOAc (10 mL × 3). The organic phase was concentrated and purified by prep-HPLC (column: Phenomenex Synergi C18 150 × 25 × 10 μm; mobile phase: [water (0.225%FA)-ACN]; B %: 65–95%, 10 min) to afford 5-(2-(1-(4-bromophenyl)-3-(4-chlorophenyl)-1*H*-pyrazol-4-yl)ethyl)-1,3,4-oxadiazol-2(3*H*)-one (**49**) as a white solid. Yield: 93 mg (34%). ¹H NMR (300 MHz, DMSO-*d*₆): δ 8.57 (s, 1H), 7.86–7.82 (m, 2H), 7.76–7.69 (m, 4H), 7.59–7.51 (m, 2H), 3.05–2.96 (m, 2H), 2.94–2.87 (m, 2H). LC/MS (APCI⁺): calculated for C₁₉H₁₄BrClN₄O₂, 444.00; observed *m/z* [M + H]⁺ 445.0; HPLC purity: 98%.

N-(5-(1,3-bis(4-chlorophenyl)-1*H*-pyrazol-4-yl)-4,5-dihydroisoxazol-3-yl)methanesulfonamide (**50**). To a solution of methanesulfonamide (250 mg, 2.63 mmol) in DMF (2 mL) was added NaH (100 mg, 2.71 mmol), and the reaction mixture was stirred for 3 min under a nitrogen atmosphere. Then, a solution of 5-(1,3-bis(4-chlorophenyl)-1*H*-pyrazol-4-yl)-3-bromo-4,5-dihydroisoxazole (**97**) (0.100 g, 0.229 mmol) in DMF (2 mL) was added, and the mixture was heated to 90 °C in a pressure tube for 16 h (Scheme S9). The cooled solution was diluted with NaHCO₃ solution (50 mL) and extracted with EtOAc (2 × 50 mL). The organic phase was dried over Na₂SO₄ and evaporated, and the material was purified by flash chromatography (Et₂O/HCOOH 99.5/0.5 to 99/1) yielding *N*-(5-(1,3-bis(4-chlorophenyl)-1*H*-pyrazol-4-yl)-4,5-dihydroisoxazol-3-yl)-methanesulfonamide (**50**) after crystallization from CH₂Cl₂/diisopropylether. Yield: 28 mg (27%). ¹H NMR (300 MHz, methanol-*d*₄): δ 8.50 (s, 1H), 7.86 (d, *J* = 9.0 Hz, 2H), 7.80 (d, *J* = 8.6 Hz, 2H), 7.55–7.47 (m, 4H), 5.71 (t, *J* = 10.0 Hz, 1H), 3.47 (dd, *J* = 16.7, 9.8 Hz, 1H), 3.31–3.24 (m, 1H), 3.21 (s, 3H). LC/MS (ESI⁺): calculated for C₁₉H₁₆Cl₂N₄O₃S, 450.03; observed *m/z* [M + H]⁺ 450.8, 452.8; HPLC purity: >99%.

■ ASSOCIATED CONTENT

SI Supporting Information

The Supporting Information is available free of charge at <https://pubs.acs.org/doi/10.1021/acs.jmedchem.1c00837>.

Synthetic schemes, synthesis of intermediates, analytical spectra for lead compounds, microbiology assays, *in vitro* DMPK assays, mouse PK studies, and *in vivo* efficacy studies (PDF)

Data from RNA microarray experiment of compound **8** (XLSX)

Data from RNA microarray experiment of compound **16** (XLSX)

Molecular formula strings and some data (CSV)

■ AUTHOR INFORMATION

Corresponding Authors

Sandeep R. Ghorpade – Drug Discovery and Development Centre (H3D), Department of Chemistry, University of Cape Town, Rondebosch 7701, South Africa; orcid.org/0000-0002-9311-1572; Phone: +27 21 650 1250; Email: Sandeep.ghorpade@uct.ac.za

Kelly Chibale – Drug Discovery and Development Centre (H3D), Department of Chemistry, University of Cape Town, Rondebosch 7701, South Africa; South African Medical Research Council Drug Discovery and Development Research Unit, Department of Chemistry and Institute of Infectious Disease and Molecular Medicine, University of Cape Town, Rondebosch 7701, South Africa; orcid.org/0000-0002-1327-4727; Phone: +27 21 650 2553; Email: kelly.chibale@uct.ac.za

Authors

Lutete Peguy Khonde – Drug Discovery and Development Centre (H3D), Department of Chemistry, University of Cape Town, Rondebosch 7701, South Africa

Rudolf Müller – Drug Discovery and Development Centre (H3D), Department of Chemistry, University of Cape Town, Rondebosch 7701, South Africa

Grant A. Boyle – Drug Discovery and Development Centre (H3D), Department of Chemistry, University of Cape Town, Rondebosch 7701, South Africa

Virsinha Reddy – Drug Discovery and Development Centre (H3D), Department of Chemistry, University of Cape Town, Rondebosch 7701, South Africa

Aloysius T. Nchinda – Drug Discovery and Development Centre (H3D), Department of Chemistry, University of Cape Town, Rondebosch 7701, South Africa

Charles J. Eyermann – Drug Discovery and Development Centre (H3D), Department of Chemistry, University of Cape Town, Rondebosch 7701, South Africa

Stephen Fienberg – Drug Discovery and Development Centre (H3D), Department of Chemistry, University of Cape Town, Rondebosch 7701, South Africa

Vinayak Singh – Drug Discovery and Development Centre (H3D), Institute of Infectious Disease and Molecular Medicine and South African Medical Research Council Drug Discovery and Development Research Unit, Department of Chemistry and Institute of Infectious Disease and Molecular Medicine, University of Cape Town, Rondebosch 7701, South Africa; orcid.org/0000-0001-9002-2489

Alissa Myrick – Drug Discovery and Development Centre (H3D), Institute of Infectious Disease and Molecular Medicine, University of Cape Town, Rondebosch 7701, South Africa

Efrem Abay – Drug Discovery and Development Centre (H3D), Division of Clinical Pharmacology, Department of Medicine, University of Cape Town, Cape Town 7925, South Africa

Mathew Njoroge – Drug Discovery and Development Centre (H3D), Division of Clinical Pharmacology, Department of Medicine, University of Cape Town, Cape Town 7925, South Africa

Nina Lawrence – Drug Discovery and Development Centre (H3D), Division of Clinical Pharmacology, Department of Medicine, University of Cape Town, Cape Town 7925, South Africa

Qin Su – Genomic Technologies Section, Research Technologies Branch, National Institutes of Health, National Institute of Allergy and Infectious Diseases, Bethesda, Maryland 20892, United States

Timothy G. Myers – Genomic Technologies Section, Research Technologies Branch, National Institutes of Health, National Institute of Allergy and Infectious Diseases, Bethesda, Maryland 20892, United States

Helena I. M. Boshoff – Tuberculosis Research Section, Laboratory of Clinical Infectious Diseases, National Institutes of Health, National Institute of Allergy and Infectious Diseases, Bethesda, Maryland 20892, United States; orcid.org/0000-0002-4333-206X

Clifton E. Barry, III – Tuberculosis Research Section, Laboratory of Clinical Infectious Diseases, National Institutes of Health, National Institute of Allergy and Infectious Diseases, Bethesda, Maryland 20892, United States

Frederick A. Sirgel – South African Medical Research Council Centre for Tuberculosis Research / DST/NRF Centre of Excellence for Biomedical Tuberculosis Research, Division of Molecular Biology and Human Genetics, Faculty of Medicine and Health Science, Stellenbosch University, Cape Town 7505, South Africa


Paul D. van Helden – South African Medical Research Council Centre for Tuberculosis Research / DST/NRF Centre of Excellence for Biomedical Tuberculosis Research, Division of Molecular Biology and Human Genetics, Faculty of Medicine and Health Science, Stellenbosch University, Cape Town 7505, South Africa

Lisa M. Massoudi – Mycobacteria Research Laboratories, Department of Microbiology, Immunology, and Pathology,

Colorado State University, Fort Collins, Colorado 80523, United States

Gregory T. Robertson – *Mycobacteria Research Laboratories, Department of Microbiology, Immunology, and Pathology, Colorado State University, Fort Collins, Colorado 80523, United States*

Anne J. Lenaerts – *Mycobacteria Research Laboratories, Department of Microbiology, Immunology, and Pathology, Colorado State University, Fort Collins, Colorado 80523, United States*

Gregory S. Basarab – *Drug Discovery and Development Centre (H3D), Department of Chemistry, University of Cape Town, Rondebosch 7701, South Africa; Drug Discovery and Development Centre (H3D), Division of Clinical Pharmacology, Department of Medicine, University of Cape Town, Cape Town 7925, South Africa;  orcid.org/0000-0001-5684-6046*

Complete contact information is available at:

<https://pubs.acs.org/10.1021/acs.jmedchem.1c00837>

Author Contributions

Chemical synthesis, compound design, and SAR expansion were led by R.M. Chemical synthesis was performed by R.M., L.P.K., G.A.B., V.R., and A.T.N. Computational and compound design support was provided by C.J.E. Pharmacophore model was developed and written by S.F. Analysis and interpretation of the biology data were done by V.S. and A.M. *In vivo* PK experiments were performed by E.A. MetID studies were performed by M.N. *In vitro* DMPK data were analyzed by N.L. Agilent microarray protocols were developed by Q.S. and T.G.M. The screening of DuPont compound library and the RNA microarray experiment were performed by H.I.M.B. MIC data were generated by H.I.M.B. High-throughput screening was conceptualized and led by C.E.B. MICs against clinical isolates were conducted by F.A.S. and P.D.v.H. Efficacy studies were planned and conducted by L.M. and G.R. Efficacy studies were guided by A.L. G.S.B. provided scientific and strategic guidance for the work and edited the manuscript. S.R.G. provided strategic support and gave inputs on the compound design. Introduction, hit identification, SAR, biology triage, and conclusion sections of the manuscript were written by S.R.G. Synthesis and chemistry experimental sections were written by L.P.K. *In vitro* and *in vivo* DMPK and efficacy sections were written by M.N. and S.R.G. and were further edited by G.R. Funding acquisition along with scientific and strategic support were done by K.C. All authors have given approval to the final version of the manuscript.

Funding

The project was funded through Global Health Grants (number OPP1066878) received from the Bill and Melinda Gates Foundation, the Division of Intramural Research of the NIAID/NIH, and the Strategic Health Innovation Partnerships (SHIP) unit of the South African Medical Research Council (SAMRC). The University of Cape Town, SAMRC and the South African Research Chairs Initiative of the Department of Science and Innovation, administered through the South African National Research Foundation, are gratefully acknowledged for support (K.C.).

Notes

The authors declare no competing financial interest.

^aA.M. deceased in November 2019.

ACKNOWLEDGMENTS

The authors acknowledge DuPont Chemicals, USA for donating the compound library. The authors thank Dr. Sridevi Bashayam, Dr. Jayanth Thiruvellore, and Rajkumar Dhinakaran from Syngene, India and the chemistry team from WuXi AppTec, China for profound chemistry support. The authors thank Tando Ntsabo and Nicole Cardoso from TB biology, H3D for performing MIC and biology triage assays. The authors thank the technical staff at *in vitro* DMPK and parasitology divisions of H3D for their excellent technical assistance in generating all *in vitro* DMPK and cytotoxicity data. The authors thank Marianna de Kock and Claudia Spies, SAMRC and Stellenbosch University, South Africa for their excellent technical assistance in generating MICs against clinical TB isolates.

ABBREVIATIONS

TB, tuberculosis; MIC, minimum inhibitory concentration; SAR, structure–activity relationship; RT, room temperature; MeOH, methanol; EtOH, ethanol; EtOAc, ethyl acetate; DIPEA, diisopropylethylamine; THF, tetrahydrofuran; DMF, *N,N*-dimethylformamide; BuOH, butanol; HATU, 1-[bis-(dimethylamino)methylene]-1*H*-1,2,3-triazolo[4,5-*b*]pyridinium 3-oxide hexafluorophosphate; POCl₃, phosphorus(V) oxychloride; SOCl₂, thionyl chloride; NaBH₄, sodium borohydride; NaCNBH₃, sodium cyanoborohydride; LAH, lithium aluminum hydride; mCPBA, *meta*-chloroperbenzoic acid; AUC, area under the curve

REFERENCES

- (1) World Health Organization *Global Tuberculosis Report*, 2019. <https://www.who.int/tb/global-report-2019> August 13, 2020.
- (2) Pontali, E.; Sotgiu, G.; D'Ambrosio, L.; Centis, R.; Migliori, G. B. Bedaquiline and multidrug-resistant tuberculosis: A systematic and critical analysis of the evidence. *Eur. Respir. J.* **2016**, *47*, 394–402.
- (3) Our Pipeline: Pretomanid. <https://www.tballiance.org/portfolio/compound/pretomanid> (April 19, 2021).
- (4) Xavier, A.; Lakshmanan, M. Delamanid: A new armor in combating drug-resistant tuberculosis. *J. Pharmacol. Pharmacother.* **2014**, *5*, 222–224.
- (5) Makarov, V.; Mikušová, K. Development of Macozinone for TB treatment: An update. *Appl. Sci.* **2020**, *10*, 2269.
- (6) Early bactericidal activity of TBA-7371 in pulmonary tuberculosis. <https://clinicaltrials.gov/ct2/show/NCT04176250> April 19, 2021.
- (7) Sacksteder, K. A.; Protopopova, M.; Barry, C. E.; Andries, K.; Nacy, C. A. Discovery and development of SQ109: A new antitubercular drug with a novel mechanism of action. *Future Microbiol.* **2012**, *7*, 823–837.
- (8) de Jager, V. R.; Dawson, R.; van Niekerk, C.; Hutchings, J.; Kim, J.; Vanker, N.; van der Merwe, L.; Choi, J.; Nam, K.; Diacon, A. H. Telacebec (Q203), a new antituberculosis agent. *N. Engl. J. Med.* **2020**, *382*, 1280–1281.
- (9) Tenero, D.; Derimanov, G.; Carlton, A.; Tonkyn, J.; Davies, M.; Cozens, S.; Gresham, S.; Gaudion, A.; Puri, A.; Muliaditan, M.; Rullas-Trincado, J.; Mendoza-Losana, A.; Skingsley, A.; Barros-Aguirre, D. First-time-in-human study and prediction of early bactericidal activity for GSK3036656, a potent leucyl-tRNA synthetase inhibitor for tuberculosis treatment. *Antimicrob. Agents Chemother.* **2019**, *63*, No. e00240.
- (10) Schechter, G. F.; Scott, C.; True, L.; Raftery, A.; Flood, J.; Mase, S. Linezolid in the treatment of multidrug-resistant tuberculosis. *Clin. Infect. Dis.* **2010**, *50*, 49–55.
- (11) Niederweis, M. Nutrient acquisition by mycobacteria. *Microbiology* **2008**, *154*, 679–692.

- (12) Warner, D. F. Mycobacterium tuberculosis metabolism. *Cold Spring Harbor Perspect. Med.* **2014**, *5*, a021121.
- (13) Wilburn, K. M.; Fieweger, R. A.; VanderVen, B. C. Cholesterol and fatty acids grease the wheels of Mycobacterium tuberculosis pathogenesis. *Pathog. Dis.* **2018**, *76*, fty021.
- (14) Brzostek, A.; Pawelczyk, J.; Rumijowska-Galewicz, A.; Dziadek, B.; Dziadek, J. Mycobacterium tuberculosis is able to accumulate and utilize cholesterol. *J. Bacteriol.* **2009**, *191*, 6584–6591.
- (15) Marrero, J.; Trujillo, C.; Rhee, K. Y.; Ehrh, S. Glucose phosphorylation is required for Mycobacterium tuberculosis persistence in mice. *PLoS Pathog.* **2013**, *9*, No. e1003116.
- (16) Martinez-Grau, M. A.; Valcarcel, I. C. G.; Early, J. V.; Gessner, R. K.; de Melo, C. S.; de la Nava, E. M. M.; Korkegian, A.; Ovechkina, Y.; Flint, L.; Gravelle, A.; Cramer, J. W.; Desai, P. V.; Street, L. J.; Odingo, J.; Masquelin, T.; Chibale, K.; Parish, T. Synthesis and biological evaluation of aryl-oxadiazoles as inhibitors of Mycobacterium tuberculosis. *Bioorg. Med. Chem. Lett.* **2018**, *28*, 1758–1764.
- (17) Gold, B.; Pingle, M.; Brickner, S. J.; Shah, N.; Roberts, J.; Rundell, M.; Bracken, W. C.; Warrier, T.; Somersan, S.; Venugopal, A.; Darby, C.; Jiang, X.; Warren, J. D.; Fernandez, J.; Ouerfelli, O.; Nuernberger, E. L.; Cunningham-Bussell, A.; Rath, P.; Chidawanyika, T.; Deng, H.; Realubit, R.; Glickman, J. F.; Nathan, C. F. Nonsteroidal anti-inflammatory drug sensitizes Mycobacterium tuberculosis to endogenous and exogenous antimicrobials. *Proc. Natl. Acad. Sci. U.S.A.* **2012**, *109*, 16004–16011.
- (18) Salunke, S. B.; Azad, A. K.; Kapuriya, N. P.; Balada-Llasat, J.-M.; Pancholi, P.; Schlesinger, L. S.; Chen, C.-S. Design and synthesis of novel anti-tuberculosis agents from the celecoxib pharmacophore. *Bioorg. Med. Chem.* **2015**, *23*, 1935–1943.
- (19) Yadlapalli, R. K.; Chourasia, O. P.; Vemuri, K.; Sritharan, M.; Perali, R. S. Synthesis and in vitro anticancer and antitubercular activity of diarylpyrazole ligated dihydropyrimidines possessing lipophilic carbamoyl group. *Bioorg. Med. Chem. Lett.* **2012**, *22*, 2708–2711.
- (20) Nardi, A.; Christensen, J.; Kejser, Jones, D. Spencer. Novel pyrazole derivatives useful as potassium channel modulators. WO2009,003,921A1, 08.01.2009, 2008.
- (21) Swiss, R.; Will, Y. Assessment of mitochondrial toxicity in HepG2 cells cultured in high-glucose- or galactose-containing media. *Curr. Protoc. Toxicol.* **2011**, *49*, 1–14.
- (22) Dixon, S. L.; Smondyrev, A. M.; Knoll, E. H.; Rao, S. N.; Shaw, D. E.; Friesner, R. A. PHASE: A new engine for pharmacophore perception, 3D QSAR model development, and 3D database screening: 1. Methodology and preliminary results. *J. Comput.-Aided Mol. Des.* **2006**, *20*, 647–671.
- (23) ACD/Labs, Release 2019.2.2, Advanced Chemistry Development, Inc: Toronto, Ontario, Canada, 2020.
- (24) Arora, K.; Ochoa-Montaño, B.; Tsang, P. S.; Blundell, T. L.; Dawes, S. S.; Mizrahi, V.; Bayliss, T.; Mackenzie, C. J.; Cleghorn, L. A. T.; Ray, P. C.; Wyatt, P. G.; Uh, E.; Lee, J.; Barry, C. E.; Boshoff, H. I. Respiratory flexibility in response to inhibition of cytochrome oxidase in Mycobacterium tuberculosis. *Antimicrob. Agents Chemother.* **2014**, *58*, 6962–6965.
- (25) Moosa, A.; Lamprecht, D. A.; Arora, K.; Barry, C. E.; Boshoff, H. I. M.; Ioerger, T. R.; Steyn, A. J. C.; Mizrahi, V.; Warner, D. F. Susceptibility of Mycobacterium tuberculosis cytochrome oxidase mutants to compounds targeting the terminal respiratory oxidase, cytochrome c. *Antimicrob. Agents Chemother.* **2017**, *61*, No. e01338.
- (26) Naran, K.; Moosa, A.; Barry, C. E.; Boshoff, H. I. M.; Mizrahi, V.; Warner, D. F. Bioluminescent reporters for rapid mechanism of action assessment in tuberculosis drug discovery. *Antimicrob. Agents Chemother.* **2016**, *60*, 6748–6757.
- (27) Ardito, F.; Posteraro, B.; Sanguinetti, M.; Zanetti, S.; Fadda, G. Evaluation of BACTEC Mycobacteria Growth Indicator Tube (MGIT 960) automated system for drug susceptibility testing of Mycobacterium tuberculosis. *J. Clin. Microbiol.* **2001**, *39*, 4440–4444.
- (28) Rowland, M. Protein binding and drug clearance. *Clin. Pharmacokinet.* **1984**, *9*, 10–17.
- (29) Varma, M. V. S.; Chang, G.; Lai, Y.; Feng, B.; El-Kattan, A. F.; Litchfield, J.; Goosen, T. C. Physicochemical property space of hepatobiliary transport and computational models for predicting rat biliary excretion. *Drug Metab. Dispos.* **2012**, *40*, 1527–1537.
- (30) Smith, D. A. Evolution of ADME science: Where else can modeling and simulation contribute? *Mol. Pharm.* **2013**, *10*, 1162–1170.
- (31) Gao, W.; Kim, J.-Y.; Anderson, J. R.; Akopian, T.; Hong, S.; Jin, Y.-Y.; Kandror, O.; Kim, J.-W.; Lee, I.-A.; Lee, S.-Y.; McAlpine, J. B.; Mulugeta, S.; Sunoqrot, S.; Wang, Y.; Yang, S.-H.; Yoon, T.-M.; Goldberg, A. L.; Pauli, G. F.; Suh, J.-W.; Franzblau, S. G.; Cho, S. The cyclic peptide ecumicin targeting ClpC1 is active against Mycobacterium tuberculosis in vivo. *Antimicrob. Agents Chemother.* **2015**, *59*, 880–889.
- (32) Cho, S. H.; Warit, S.; Wan, B.; Hwang, C. H.; Pauli, G. F.; Franzblau, S. G. Low-oxygen-recovery assay for high-throughput screening of compounds against nonreplicating. *Antimicrob. Agents Chemother.* **2007**, *51*, 1380–1385.
- (33) Akester, J. N.; Njaria, P.; Nchinda, A.; Le Manach, C.; Myrick, A.; Singh, V.; Lawrence, N.; Njoroge, M.; Taylor, D.; Moosa, A.; Smith, A. J.; Brooks, E. J.; Lenaerts, A. J.; Robertson, G. T.; Ioerger, T. R.; Mueller, R.; Chibale, K. Synthesis, structure–activity relationship, and mechanistic studies of aminoquinazolinones displaying antimycobacterial activity. *ACS Infect. Dis.* **2020**, *6*, 1951–1964.
- (34) Ray, P. C.; Huggett, M.; Turner, P. A.; Taylor, M.; Cleghorn, L. A. T.; Early, J.; Kumar, A.; Bonnett, S. A.; Flint, L.; Joerss, D.; Johnson, J.; Korkegian, A.; Mullen, S.; Moure, A. L.; Davis, S. H.; Murugesan, D.; Mathieson, M.; Caldwell, N.; Engelhart, C. A.; Schnappinger, D.; Epemolu, O.; Zuccotto, F.; Riley, J.; Scullion, P.; Stojanovski, L.; Massoudi, L.; Robertson, G. T.; Lenaerts, A. J.; Freiberg, G.; Kempf, D. J.; Masquelin, T.; Hipskind, P. A.; Odingo, J.; Read, K. D.; Green, S. R.; Wyatt, P. G.; Parish, T. Spirocyclic MmpL3 inhibitors with improved hERG and cytotoxicity profiles as inhibitors of Mycobacterium tuberculosis growth. *ACS Omega* **2021**, *6*, 2284–2311.
- (35) Oh, S.; Park, Y.; Engelhart, C. A.; Wallach, J. B.; Schnappinger, D.; Arora, K.; Manikkam, M.; Gac, B.; Wang, H.; Murgolo, N.; Olsen, D. B.; Goodwin, M.; Sutphin, M.; Weiner, D. M.; Via, L. E.; Boshoff, H. I. M.; Barry, C. E. Discovery and structure–activity-relationship study of N-alkyl-5-hydroxypyrimidinone carboxamides as novel antitubercular agents targeting decaprenylphosphoryl- β -d-ribose 2'-oxidase. *J. Med. Chem.* **2018**, *61*, 9952–9965.
- (36) Singh, V.; Donini, S.; Pacitto, A.; Sala, C.; Hartkoorn, R. C.; Dhar, N.; Keri, G.; Ascher, D. B.; Mondésert, G.; Vocat, A.; Lupien, A.; Sommer, R.; Vermet, H.; Lagrange, S.; Buechler, J.; Warner, D. F.; McKinney, J. D.; Pato, J.; Cole, S. T.; Blundell, T. L.; Rizzi, M.; Mizrahi, V. The inosine monophosphate dehydrogenase, Guab2, is a vulnerable new bactericidal drug target for tuberculosis. *ACS Infect. Dis.* **2017**, *3*, 5–17.
- (37) Boshoff, H. I. M.; Myers, T. G.; Copp, B. R.; McNeil, M. R.; Wilson, M. A.; Barry, C. E. The transcriptional responses of Mycobacterium tuberculosis to inhibitors of metabolism: Novel insights into drug mechanisms of action. *J. Biol. Chem.* **2004**, *279*, 40174–40184.
- (38) Schrödinger Release 2020-2, Maestro, Schrödinger2020-2: New York, NY, 2020.